

Paving the Road to the Habitable Worlds Observatory with High-Resolution Imaging I: New and Archival Speckle Observations of Potential HWO Target Stars

ZACHARY D. HARTMAN,¹ CATHERINE A. CLARK,² MICHAEL B. LUND,² KATHRYN V. LESTER,³ JOSÉ A. CABALLERO,⁴ STEVE B. HOWELL,¹ DAVID CIARDI,² SARAH DEVENY,⁵ MARK E. EVERETT,⁶ ELISE FURLAN,² VENU KALARI,⁷ COLIN LITTLEFIELD,⁵ ANDREW W. STEPHENS,⁷ JENNIFER A. BURT,⁸ GUILLAUME HUBER,⁹ RACHEL MATSON,¹⁰ ERIC E. MAMAJEK,⁸ AND NOAH TUCHOW¹¹

¹*NASA Ames Research Center, Moffett field, CA 94035, USA*

²*NASA Exoplanet Science Institute, IPAC, California Institute of Technology, Pasadena, CA 91125, USA*

³*Mount Holyoke College, South Hadley MA 01075, USA*

⁴*Centro de Astrobiología (CSIC-INTA), ESAC, Camino bajo del castillo s/n, 28692 Villanueva de la Cañada, Madrid, Spain*

⁵*Bay Area Environmental Research Institute, Moffett Field, CA 94035, USA*

⁶*NSF NOIRLab, 950 N. Cherry Ave., Tucson, AZ 85719, USA*

⁷*International Gemini Observatory/ NSF NOIRLab, 670 A'ohoku Place, Hilo, HI 96720, USA*

⁸*Jet Propulsion Laboratory, California Institute of Technology, 4800 Oak Grove Drive, Pasadena, CA 91109, USA*

⁹*Institute for Astronomy, University of Hawai'i, 640 N. Aohoku Place, Hilo, HI 96720, USA*

¹⁰*U.S. Naval Observatory, 3450 Massachusetts Ave. NW, Washington, D.C. 20392, USA*

¹¹*NASA Goddard Space Flight Center, Greenbelt, Maryland, USA*

ABSTRACT

One of the key goals of the Habitable Worlds Observatory (HWO) is to directly image about 25 potentially habitable exoplanets and determine their properties. This challenge will require a large survey of nearby, bright stars – ~ 100 according to the Astro2020 Decadal Survey. To ensure the success of the mission and to help guide design decisions, the stellar multiplicity of the target stars must be well-understood. To this end, we present optical speckle imaging of stars in the NASA Exoplanet Exploration Program (ExEP) provisional HWO star list, which is currently the Tier 1 target list for the HWO Target Stars and Systems Sub-Working Group. We obtained new observations using ‘Alopeke and Zorro at Gemini Observatory and queried the Exoplanet Follow-up Observing Program Archive for archival observations, resulting in speckle imaging data for 80 of the 164 stars. We confirmed one candidate companion detected previously by Gaia (HD 90089) and obtained an ambiguous detection of a known companion (HD 212330). To examine our sensitivity to companions, we simulated stellar companions down to $\sim 0.1M_{\odot}$ for each target and found that 75%-85% would be detected in our speckle images; the remaining simulated companions are either too faint or too close-in, and will require follow-up using other methods such as long-term spectroscopic measurements and space-based techniques. This work represents a first step towards surveying potential HWO targets for close-in stellar companions and helping to inform the target selection process for the HWO direct-imaging survey, bringing us closer towards the discovery of potential habitable worlds.

Keywords: Stellar astronomy (1583) — Observational astronomy (1145) — Multiple stars (1081) — Exoplanet astronomy (486)

1. INTRODUCTION

The Astro2020 Decadal Survey laid out a grand vision for the field of astronomy over the coming decades (of Sciences Engineering & Medicine 2021). One of its key recommendations called for NASA to begin planning a new Infrared/Optical/Ultraviolet (IR/O/UV) space mission for launch in the mid-2040s. Currently called the Habitable

Worlds Observatory (HWO), one of the mission’s primary goals is to directly image 25 potentially habitable exoplanets. Now, NASA and the astronomical community are beginning to prepare for HWO in a variety of ways, including maturing technology (Scowen et al. 2025) and developing scientific working groups¹ to inform the final design of the telescope and the target sample. For the direct-imaging survey, this preparation means beginning the process of assembling a large sample of nearby, bright stars with well-defined properties – such as mass, age, and radius – from which future scientists will determine the targets most amenable to a search for habitable-zone planets.

As a part of this process, the HWO target star candidates will need to be searched for close stellar companions. Although the definition of “close” in multiple stellar systems is fluid and context-dependent, as described in Cifuentes et al. (2025), for this study, close means companions with angular separations $< 3''$, or projected physical separations ≤ 30 au for typical target distances of ~ 10 pc. This separation limit matches that of Mamajek & Stapelfeldt (2024) and was selected as a reasonable limit for what HWO’s starlight suppression techniques might be able to take into account. Roughly half of solar-type stars (F-, G-, and early K-dwarfs) are expected to form in multi-star systems (Duquennoy & Mayor 1991; Raghavan et al. 2010; Duchêne & Kraus 2013; Tokovinin 2014; Offner et al. 2023). Unbound chance alignments, where one or more stars appear in the background and are unassociated, are also possible. From a technical perspective, these additional stars – bound or unbound – will add more light into the field-of-view, increasing the noise in the observations and potentially over-powering the light from any planets in the system. However, advances in multi-star wavefront control may allow HWO to reach the necessary noise floor to detect potentially habitable exoplanets, even in the presence of a close-in stellar companion (Belikov et al. 2015; Thomas et al. 2015; Sirbu et al. 2017, 2023; Bendek et al. 2021). From a scientific perspective, bound companions with separations less than 100 au may truncate or inhibit the formation of disks around the stars in the system, or gravitationally excite and eject planetesimals, preventing the formation of the planets HWO is hoping to observe (Quintana & Lissauer 2006; Haghighipour & Raymond 2007; Jang-Condell 2015; Rafikov & Silsbee 2015a,b; Thebault & Haghighipour 2015; Hamers et al. 2021). As such, it has been shown that the stellar companions in planet-hosting systems are shifted to larger separations as compared to field multiples (Kraus et al. 2016; Lester et al. 2021; Clark et al. 2022; González-Payo et al. 2024). Nonetheless, while the likelihood of finding planets in close binaries is lower than around single stars, it has been shown that multi-star systems with separations less than 100 au can host planets (Zucker et al. 2004; Bohn et al. 2020; Matson et al. 2019; Feng et al. 2022; González-Payo et al. 2024; Sullivan et al. 2024). On the other hand, wide stellar systems with separations of 10s to 100s of arcseconds and larger may be especially valuable for HWO as the wide companion would not interfere with the direct imaging observation, but could provide a wealth of information on the system ranging from the metallicity, age, or formation scenarios depending on the nature of the companion (Tokovinin 2017; Hawkins et al. 2020; Heintz et al. 2024).

To ensure the success of the mission, potential HWO targets must be searched for close-in stellar companions with periods of days to decades, either to remove the binaries from the target list, or to identify and characterize them for proper observation with HWO. Additionally, observations examining the area where these stars will be in 2040 to identify potential background stars and determine what effect, if any, they would have on HWO observations are needed. Multiplicity information will need to be gathered using a number of different methods, including long-term spectroscopic measurements and space-based techniques (Baroch et al. 2018; Hutter et al. 2019; Hirsch et al. 2021; Moe & Kratter 2021). However, while long-term spectroscopic observations, and subsequent radial velocity measurements, are sensitive to companions with separations less than 20 - 50 milliarcseconds, the detection sensitivity decreases significantly for systems with larger separations (Teske et al. 2015). Even space-based observatories can miss close-in companions. Gaia, for example, typically cannot resolve relatively faint companions closer than $0.6''$ - $0.8''$ as the resolution power strongly depends on the magnitude difference between the two stars (Clark et al. 2024a; Cifuentes et al. 2025; Matson et al. 2025).

Ground-based, high-resolution imaging, however, is sensitive to subarcsecond companions at moderate contrasts after only a single visit. In particular, optical speckle imaging on the 8.1-meter Gemini telescopes offers some of the highest angular resolutions ($0.025''$ at 832 nm) and largest magnitude contrasts at small separations (4-5 magnitudes at $0.1''$) of any telescope and instrument combination currently available. This allows astronomers to search for faint companions across a wide range of possible separations quickly and efficiently. As such, high-resolution imaging will play a key role in surveying the environments around potential HWO target stars, as well as characterizing the orbital parameters of any close-in binaries.

¹ <https://science.nasa.gov/astrophysics/programs/habitable-worlds-observatory/wgs/>

Over the past decade, the astronomical community has obtained, reduced, and published a large amount of data on nearby stars that may become HWO targets. In this paper, we publish new observations that were taken using the ‘Alopeke and Zorro speckle imagers. We also examine a set of high-resolution imaging data that is publicly available on the NASA Exoplanet Follow-up Observing Program (ExoFOP) archive. In Section 2, we show our new observations were obtained, how we retrieved the archival data, and how the archival observations were originally collected. We also highlight our Gaia and Washington Double Star catalog cross-matches and our literature searches for more companions. In Section 3, we present our overall results and notes on individual systems, as well as an analysis of potential companions that may be missing from our observations. In Section 4, we compare our 20- and 60-ms observations and discuss the implications of our results on target selection for HWO. We present our conclusions in Section 5.

2. METHODS

2.1. *Sample Selection*

Our sample is based on the NASA Exoplanet Exploration Program (ExEP) provisional star list for HWO (Mamajek & Stapelfeldt 2024), which consists of 164 stars. The selection for the ExEP list was based on a number of criteria, including the potential star-planet brightness ratios, the possible albedoes of the planets, the magnitude of the potential planets, the angular size of the habitable zone, and the stellar multiplicity of the systems. In particular, Mamajek & Stapelfeldt (2024) removed all systems with known companions within $3''$ that are listed in the Washington Double Star Catalog (WDS; Mason et al. 2001), as well as any spectroscopic binaries that are listed in the Ninth Catalogue of Spectroscopic Binary Orbits (SB9; Pourbaix et al. 2004). However, while extensive, neither catalog is complete to all separations or magnitude differences, and the observations are not uniform across all targets. In particular, many of the observations in the WDS were taken using small telescopes or antiquated techniques and therefore, some stellar companions may have been missed. A uniform multiplicity study, using the best available facilities, is needed for a full understanding of the stellar multiplicity of the targets on the ExEP list.

As such, we obtained new speckle observations of stars and sought out archival speckle observations of stars on the ExEP provisional star list for HWO. Table 1 includes the TESS Input Catalog (TIC, Stassun et al. 2019; Paegert et al. 2021) ID, Gaia DR3 ID, Simbad Name, R.A., decl., $\mu_{R.A.}$, $\mu_{decl.}$, Parallax, Gaia G Magnitude, Gaia $G - G_{RP}$ color, and Gaia radial velocity (V_r) for each star targeted in this study. Figure 1 shows a color-magnitude diagram of the targets surveyed throughout this work as compared to other stars within 100 pc.

2.2. *Archival and New Speckle Imaging*

We observed 34 stars using ‘Alopeke and Zorro on the 8.1-meter Gemini North and South telescopes, respectively (Scott et al. 2021). We note that one target, HD 95735, has two TIC IDs associated with it, TIC 166646191 and TIC 353969903. We take any observations associated with either of the entries to be of HD 95735 and use TIC 166646191 as the TIC ID used in this study. Four of these 34 were listed in Appendix E of Mamajek & Stapelfeldt (2024). These Appendix E targets are listed in the WDS as potential binaries, but subsequent studies have cast doubt on that determination. We therefore sought to clarify the multiplicity of these systems.

We also cross-matched the 164 targets on the ExEP provisional star list for HWO with the ExoFOP archive to search for publicly available high-resolution imaging data². Of them, 46 systems had been previously observed with either ‘Alopeke or Zorro or the NN-Explore Exoplanet Stellar Speckle Imager (NESSI) on the 3.5-meter Wisconsin-Indiana-Yale-NOIRLab (WIYN) telescope (Scott & Howell 2018). In this work, we focused on observations from these instruments as they are nearly identical, and they offer high angular resolution and large magnitude contrasts at small separations.

The observing procedure was roughly the same for each of the ‘Alopeke, Zorro, and NESSI archival observations. Speckle imaging observations consist of data cubes containing one thousand 40-ms (WIYN) or 60-ms (Gemini) exposures. These exposure times were selected in order to obtain the best signal-to-noise ratio (S/N) for the observations (Howell et al. 2011). These short exposure times allow one to “freeze” the atmospheric interference. The number of data cubes is determined either by the PI or by the on-site observer following the tables on the ‘Alopeke and Zorro³ or NESSI⁴ webpages, and depends on the magnitude of the target and weather conditions during the observation. During

² <https://exofop.ipac.caltech.edu/tess/>

³ <https://www.gemini.edu/instrumentation/lopeke-zorro>

⁴ <https://www.wiyn.org/Instruments/nessi/>

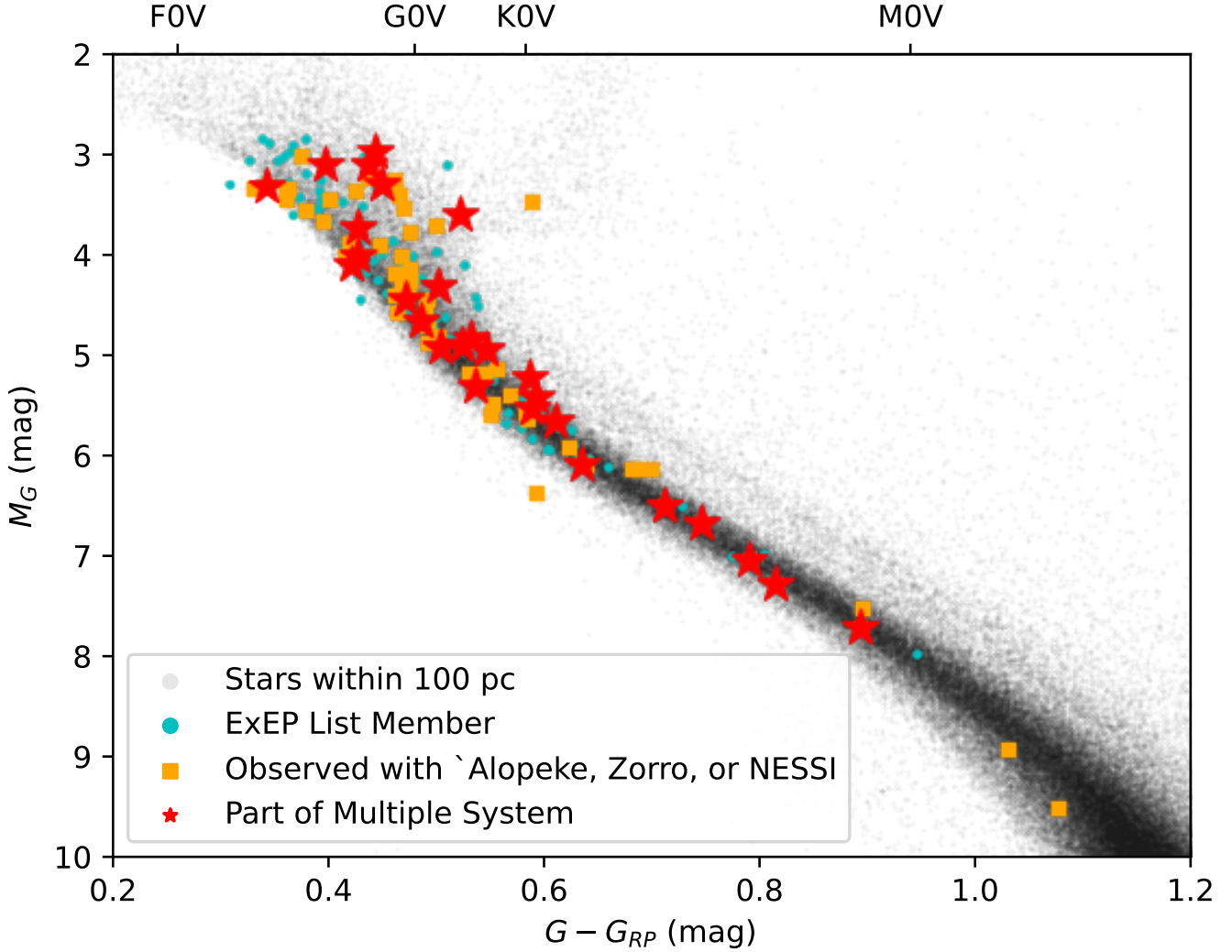


Figure 1. Color-magnitude diagram showing the targets in the ExEP target list for HWO. The grey points represent a sample of stars within 100 pc taken from Gaia DR3. The cyan points indicate the locations of the [Mamajek & Stapelfeldt \(2024\)](#) targets that are in Gaia and have not been observed with speckle imaging. Orange squares highlight 80 ExEP list targets that have ‘Alopeke, Zorro, or NESSI’ observations. Red stars show the 27 targets that have been identified as members of stellar multiples by this work. The top axis provides approximate $G - G_{RP}$ values for F0V, G0V, K0V, and M0V stars.

observations, a dichroic splits the collimated beam of light at ~ 700 nm and directs it through two filters wheels and onto two EMCCDs. For the archival observations, the 562/54 nm and 832/40 nm narrowband filters were used ($\bar{\lambda}/\Delta\lambda$). A point source standard is observed close on-sky and in-time to the target to provide an estimate of what the point spread function of a single star is in roughly the same conditions as the science was taken in. Additionally, calibration binaries are observed periodically to determine the pixel scale and image orientation of the instrument. These binaries are drawn from the Sixth Catalog of Orbits of Visual Binary Stars and are required to have grades 1 or 2 [Hartkopf et al. \(2001\)](#).

For our new observations, we modified this observing procedure in two ways. We first reduced the ‘Alopeke and Zorro’ exposure times to 20 ms rather than 60 ms to avoid potential saturation from these bright targets ($G \sim 3 - 7$ mag). We also used double the recommended amount of time on-target (six minutes) to improve the S/N of the observations and thus the contrasts achieved. In two instances, HD 5015 and the November 2024 observation of HD 88230, we observed for the normal amount of time (three minutes). We discuss the implications of using a shorter exposure time in Section 4.1.

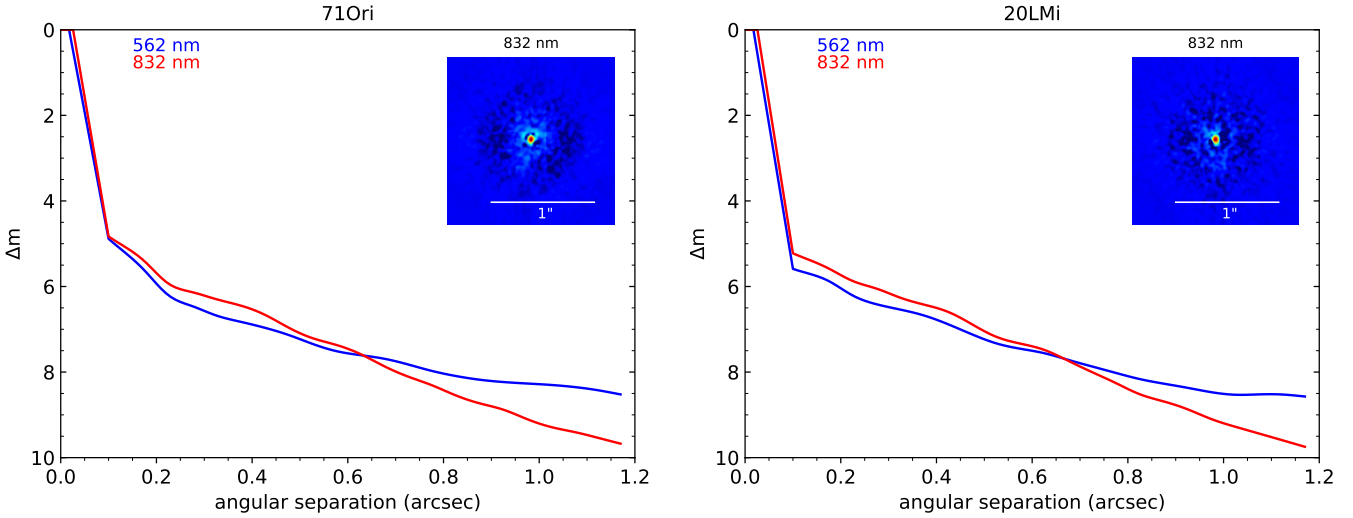


Figure 2. The contrast curves for the two narrowband filters centered at 562 nm (blue line) and 832 nm (red line) for our observation of 71 Ori and 20 LMi using ‘Alopeke at Gemini North. The insets are the reconstructed images at 832 nm.

The speckle data sets were reduced using the data reduction pipeline detailed in Horch et al. (2009, 2011a,b) and Howell et al. (2011). This pipeline uses bi-spectral analysis to compute a reconstructed image for each target (Lohmann et al. 1983). Briefly, the pipeline produces a co-added power spectrum from the speckle frames. After dividing by the power spectrum of the point source standard, fringes in the power spectrum indicate the presence of a stellar companion. The fringes are fit using a cosine-squared function to determine the angular separation (ρ), position angle (θ), and an estimate of the magnitude difference (Δm) for the companion. The reconstructed image is then generated from the modulus of the object given in the power spectrum.

Uncertainties on these properties are not provided by the pipeline for each individual target. Instead, Scott et al. (2021) analyzed a sample of calibration binaries and found a pixel scale uncertainty of 0.21 mas/pixel, position angle uncertainty of 0.7° , and magnitude difference uncertainties of 0.02 and 0.04 mag in the 562 nm and 832 nm filters. We use these as our uncertainties on ρ , Δm , and θ .

Magnitude contrast curves for both filters are then constructed by examining the maximum and minimum background values in annuli centered on the primary star. The detection limit within each annulus is estimated as the mean value of the maxima plus five times the average standard deviation of the maxima and minima. These curves assess the sensitivity of the observation to stellar companions as measured in magnitudes fainter than the primary star and as a function of angular separation. Two examples of the reconstructed images and contrast curves produced by this pipeline are shown in Figure 2. These contrast curves demonstrate that we are sensitive to stellar companions that are much fainter and redder than their host star, down to the diffraction limit of the telescope. All reconstructed images and contrast curves from the new observations are publicly available on the ExoFOP archive.

Table 2 provides results of the speckle observations and gives the TIC ID, instrument used, and PI of each observation, as well as the contrasts reached at $0.1''$ and $0.5''$ in the 562 nm and 832 nm filters. The ρ , Δm , and θ of any detected companions in the 832 nm filter are provided in Table 3. Only the 832 nm filter results are shown because no companion was detected in the 562 nm filter. We note that three multiple systems have speckle observations of both components: 61 Cyg A and B, ζ^{01} Ret and ζ^{02} Ret, and ξ Boo and ξ Boo B.

We also investigate the physical separation space probed by these observations. The left panel of Figure 3 shows the $5 - \sigma$ contrast curves for each of the stars examined in this work as blue (562 nm) and red (832 nm) lines for both Gemini and WIYN. We also provide two additional curves (cyan and orange for the 562 nm and 832 nm filters, respectively), which highlight our ‘Alopeke’s and Zorro’s sensitivity using previous companion detections over the past decade. Critically, these curves show that our observations could detect binaries down to the diffraction limit of Gemini with $\Delta m \sim 4 - 5$ mag. The right panel of Figure 3 highlights the range of projected physical separations, $\rho = \text{angular separation} * \text{distance}$, that our speckle observations are sensitive to as a function of distance to the target. The magenta bars show the limits for each target. We set the lower limit of the physical separation range to be

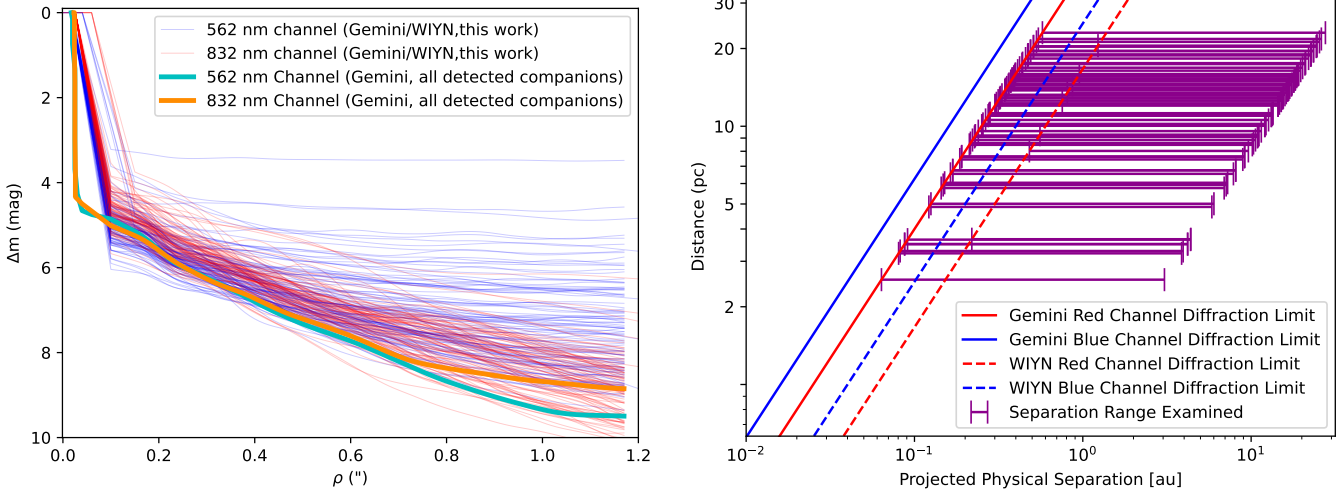


Figure 3. *Left:* Contrast curves for the 80 HWO targets surveyed in this work. The 562 nm and 832 nm contrast curves are shown as blue and red lines, respectively. The solid cyan and orange lines represent a fit to the envelope of binaries detected by ‘Alopeke and Zorro and listed on ExoFOP. These contrast curves show that we detect stellar companions that are fainter than their primaries by 4-5 magnitudes at the diffraction limits of the telescopes. *Right:* The projected physical separation range surveyed by our speckle observations for each target, shown as magenta bars. Solid and dashed lines represent the diffraction limits for the 562 nm (blue) and 832 nm (red) filters at Gemini (‘Alopeke and Zorro) and WIYN (NESSI). This figure shows that speckle imaging surveys a necessary parameter space in the search for potential companions.

the diffraction limit of the red channel at Gemini or WIYN: 0.025'' and 0.06'', respectively. The upper limit is 1.2'', above which the speckles start to de-correlate and the sensitivity to stellar companions decreases. The diagonal lines represent the diffraction limits for the 562 nm (blue) and 832 nm (red) filters.

2.3. Gaia Search

We also cross-matched our sample of 80 stars with the Gaia Catalogue of Nearby Stars (GCNS; [Gaia Collaboration et al. 2021a](#)) and [El-Badry et al. \(2021\)](#) to identify pairs of stars close on-sky with similar proper motions and parallaxes using the astrometric information provided by Gaia early Data Release 3 ([Gaia Collaboration et al. 2016, 2021b](#)). Since these are nearby targets, substantial visual motion may occur between the components of these systems over the coming years; as such, identifying these common-proper-motion (CPM) pairs is critical.

Gaia Data Release 3 (DR3) also contains useful indicators of stellar multiplicity even when a companion is unresolved ([Gaia Collaboration et al. 2023a](#)). We therefore cross-matched our sample of 80 targets with Gaia DR3 and retrieved known binary indicators ([Gaia Collaboration et al. 2023b](#)). These indicators include the Reduced Unit Weight Error (RUWE), IPD_gof_harmonic_amplitude (IPD_gof), rv_chisq_pvalue (RV_chi), rv_renormalized_gof (RV_gof), radial_velocity_error, IPD_frac_multi_peak (IPD_fmp), rv_nb_transits (RV_nb), and the Non_Single_Star flag (NSS, [Gaia Collaboration et al. 2023a](#)). RUWE is an indicator of how good the Gaia astrometric fit is to a single star model, ipd_gof_harmonic_amplitude is a measure of how much the IPD goodness-of-fit changes as a function of scan position angle, IPD_fmp is the fraction of Gaia windows where a second peak is detected, RV_chi gives the p-value of the measured RVs from Gaia, RV_gof highlights the goodness-of-fit of the radial velocities, RV_nb is the number of transits used to obtain the radial velocity, radial_velocity_error is the error in the measured radial velocity, and the NSS flag shows which targets have available information in the Gaia NSS tables. The NSS tables contain binary information on the astrometric, acceleration, and spectroscopic binaries that the Gaia mission has identified and characterized ([Gaia Collaboration et al. 2023a](#)). Table 4 provides the TIC ID, Gaia DR3 ID, R.V. Error, RUWE, IPD_fmp, whether the star is flagged as a non-single star, IPD_gof, RV_gof, RV_chi, RV_nb, and the source, Gaia ID, separation, and magnitude differences in Gaia *G* of any companion(s) found in our wide binary search.

To flag a star as a potential multiple, we start with the criteria outlined by [Cifuentes et al. \(2025\)](#). We then modified the criteria in two ways. First, we did not check the duplicated_source parameter, as [Cifuentes et al. \(2025\)](#) indicated that this is a secondary parameter rather than a primary parameter. This parameter flags sources that may have issues with astrometric quality, lack some data, or where Gaia may have detected multiple sources ([Cifuentes et al.](#)

2025). As this covers a wide range of possible issues, we do not check it as the other criteria are better at identifying stellar multiples. Second, we lowered the IPD_fmp cut to 2 following [Tokovinin \(2023\)](#). Our modified criteria are:

- $\text{RUWE} > 2$
- $\text{ipd_gof_harmonic_amplitude} > 0.1 \ \& \ \text{RUWE} > 1.4$
- $\text{ipd_frac_multi_peak} > 2$
- $\text{rv_chisq_pvalue} < 0.01 \ \& \ \text{rv_renormalized_gof} > 4 \ \& \ \text{rv_nb_transits} \geq 10$
- $\text{radial_velocity_error} \geq 10 \text{ km s}^{-1}$
- $\text{non_single_star flagged}$

Figure 4 shows the RUWE values for the 80 targets in this study as a function of their Gaia G magnitude, with the 19 targets that were flagged by the Gaia multiplicity criteria described above shown as cyan stars. We note that at $G \sim 4.5$ mag, the RUWE values begin to rise. While this could indicate the presence of an unresolved companion, it is more likely that the brightness of these targets increases the astrometric errors, leading to larger RUWE values. To demonstrate this effect, we also plot a sample of stars within 100 pc from Gaia. Therefore, the RUWE value may be unreliable for stars brighter than $G \sim 4.5$ mag. As such, unless the target is flagged as a NSS by Gaia or a companion is found via other techniques, we consider the star to be single. However, we do mark stars with these elevated Gaia metrics in Table 5, meaning one or some of the criteria above are met.

2.4. Literature Search

We searched several other sources for additional stellar companions, and to confirm companions found in our speckle images or in Gaia. The WDS was used as a starting point. In most cases, the WDS entry is confirmed; however, in some cases notes in the WDS indicated that the companion may not be bound, or the detection is spurious. In particular, we disregard systems where components included a U, S, X and/or L notes. From the WDS, U means that the pair is non-physical due to mismatched proper motions, S indicates that the components in the system have statistically different parallaxes and proper motions, X highlights a system that is a “Dubious Double,” and L indicates a linear solution.

We also examined [Golovin et al. \(2023\)](#), [Kirkpatrick et al. \(2024\)](#), [González-Payo et al. \(2024\)](#), and [González-Payo et al. \(2025\)](#) to identify any additional companions. [Golovin et al. \(2023\)](#) and [Kirkpatrick et al. \(2024\)](#) were both wide censuses of nearby stars with [Golovin et al. \(2023\)](#) going to 25 pc and [Kirkpatrick et al. \(2024\)](#) going to 20 pc. [González-Payo et al. \(2024\)](#) and [González-Payo et al. \(2025\)](#) were targeted multiplicity searches with [González-Payo et al. \(2024\)](#) focused on exoplanet-hosting stars within 100 pc and [González-Payo et al. \(2025\)](#) examining the multiplicity of stars within 10 pc.

3. RESULTS

Table 5 summarizes the results from our speckle observations, the Gaia analysis, and the literature search. We provide the TIC ID, WDS ID, whether the star is part of a Gaia CPM pair, whether the star is flagged as a possible close binary by Gaia indicators, whether the star is binary in our speckle observations, the literature source(s) primarily used to make the multiplicity determination in addition to the speckle observations and Gaia data, the multiplicity status of the star after our analysis, and any notes on the system. Figure 5 shows the projected physical separations of the multi-star systems that were identified in our analysis, with comparisons to the diffraction limits of the instruments and the selection criteria used in the ExEP provisional star list for HWO.

Overall, 27 of the 80 stars examined in this study were found to be members of multi-star systems. We identified a new stellar companion to HD 90089 (Section 3.1), and we obtained an additional speckle observation of the known companion to HD 212330 (Section 3.2). In total, we find 33 possible companions with 24 common proper motion companions, two Gaia non-single stars, including one confirmed by our speckle observations, one potential speckle detection of a known companion, and five other companions listed in the literature. We discuss known and potentially new triple systems in Section 3.3, and assess potentially missed companions in Section 3.4.

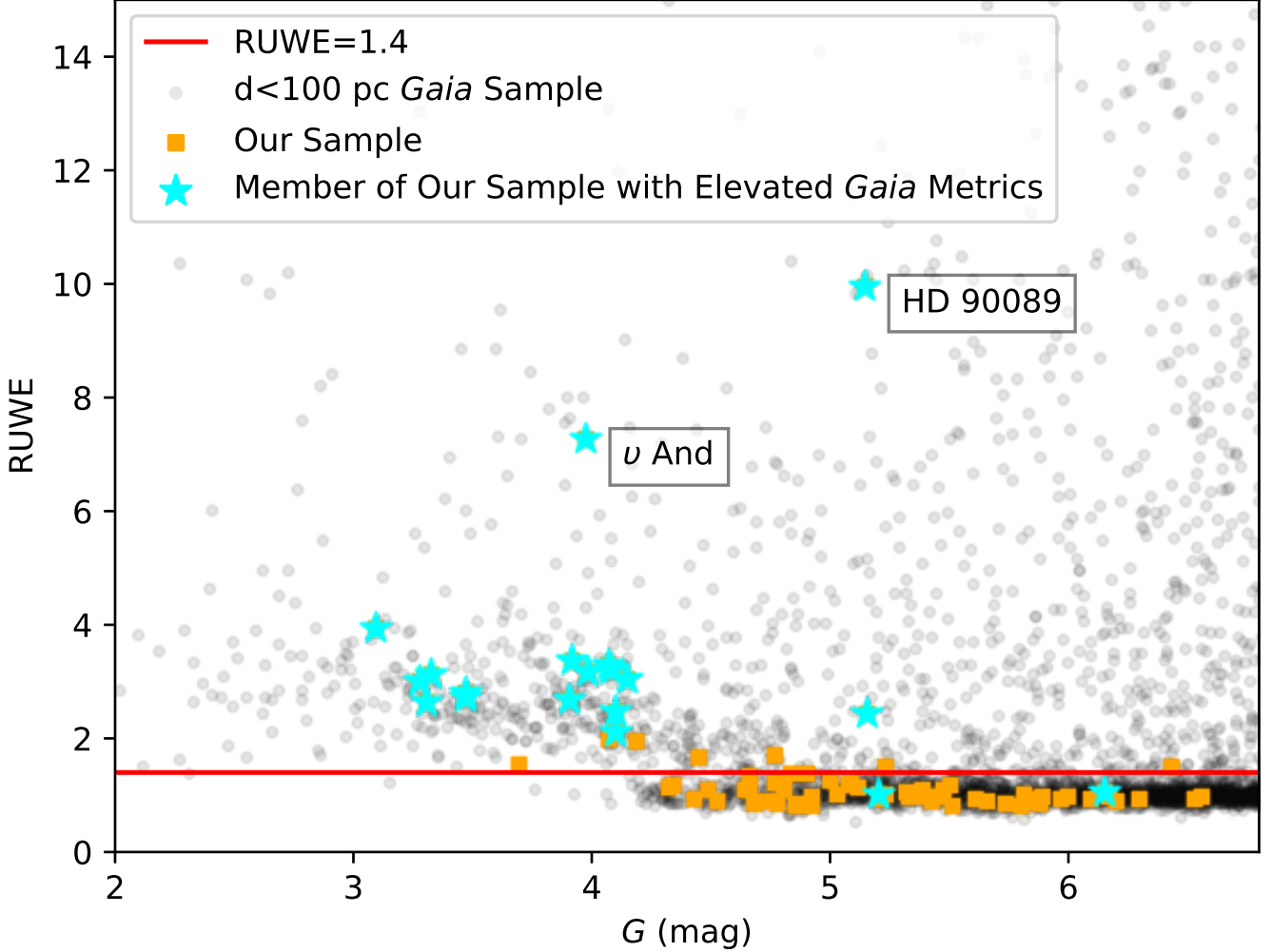


Figure 4. RUWE values of the 80 HWO targets surveyed in this work as a function of Gaia G magnitude. Cyan stars indicate the 19 stars that were flagged as potential binaries by our Gaia metric criteria, while the remaining 61 stars are shown as orange squares. The red line indicates a RUWE value of 1.4, which is the value typically used to distinguish single and non-single stars. The black points represent a sample of stars within 100 pc from Gaia DR3. We label the two stars with $\text{RUWE} > 7$. As one goes to brighter magnitudes, the RUWE values rise, which could indicate the presence of unresolved companions. However, it is more likely that the brightness of these targets is increasing the astrometric errors. As such, the RUWE value may not be the best indicator of stellar multiplicity for stars brighter than $G \sim 4.5$ mag.

3.1. HD 90089/TIC 367631379

HD 90089 is a F4V star and is ~ 23 pc away. An examination of the literature data on Simbad shows few adaptive optics or speckle imaging observations of this star. The most recent was [McAlister et al. \(1989\)](#) using speckle imaging on the 4-m Mayall Telescope at Kitt Peak National Observatory. No companion was detected in those observations.

We detect a companion to HD 90089 at 832 nm, with a separation of $0.022''$, a position angle of 2.4° , and a magnitude difference of 0.45. The companion is not detected at 562 nm. This system was already known to be multiple, with a companion at $13.5''$ noted in the WDS ([Gatewood & Gatewood 2016](#)) and [El-Badry et al. \(2021\)](#). We note that the $0.022''$ separation is below the nominal diffraction limit of the speckle instruments at Gemini Observatory; however, speckle imaging can go beyond this limit ([Horch et al. 2011b](#)). This target also has elevated Gaia multiplicity metrics (e.g., $\text{RUWE}=9.9$) that provides more evidence towards the detected companion being real.

HD 90089 is also marked as a Gaia non-single star, and has an astrometric orbit listed in Gaia DR3. To examine if our detection and the Gaia detection are one in the same, we used the orbital parameters from the Gaia orbit and

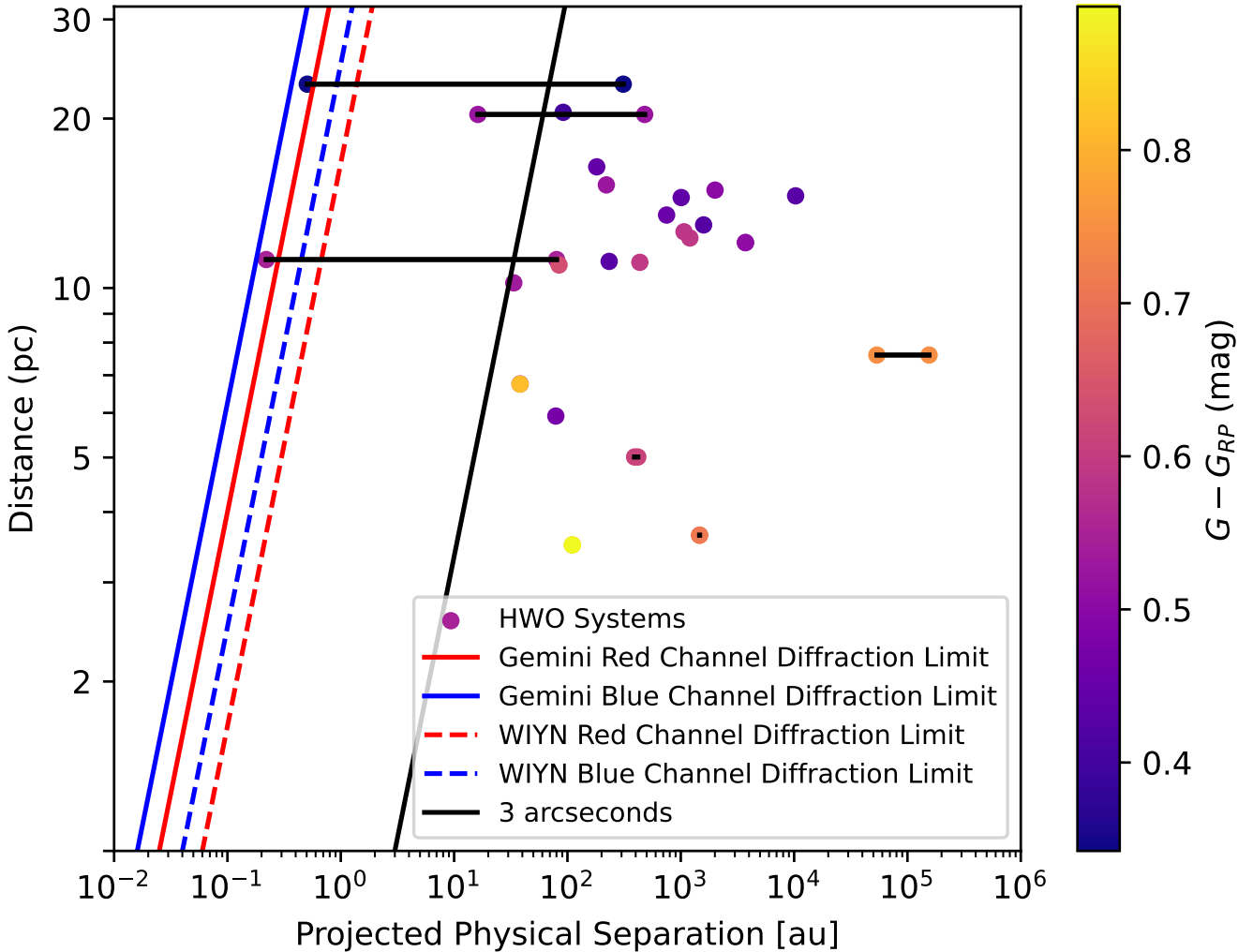


Figure 5. Distances to the 27 multi-star systems identified in this study as a function of projected physical separation. The solid red and blue lines represent the nominal diffraction limits for the 562 nm (blue) and 832 nm (red) filters installed in ‘Alopeke and Zorro. The dashed lines represent the same for NESSI. The black line is the $3''$ cut used in the original sample selection for the ExEP provisional star list for HWO. The color of the points highlights the $G - G_{RP}$ values of the stars. If the system is triple, then it has two points representing the AB and AC components and we connect these systems by the black horizontal lines. We assume the primary’s distance as the distance for the system. The majority of the stellar companions lie beyond $3''$, which shows that the selection criteria from [Mamajek & Stapelfeldt \(2024\)](#) removed most close-in multiples from the sample. However, some systems are still found with separations less than $3''$, which highlights the need for a uniform multiplicity study of all the potential HWO target stars.

the NSS Tools programs⁵ to determine where in the orbit the stellar companion would have been at the time of our observations ([Halbwachs et al. 2023](#)). This analysis put the companion at a separation of $0.024''$ at the time of our speckle observations, which is within the errors of our measurement. However, our analysis predicted the companion would be at a position angle of 260.9° , which is different than our result.

In speckle imaging, there is the potential for a 180° ambiguity in position angle due to the phase not being well constrained. This is caused by either the faintness of the companion resulting in low S/N, and thus a lack of phase information, or a close-in companion resulting in few fringes to fit during the analysis. As such, we re-ran this analysis with a 180° position angle offset from our measurement (i.e., 182.4°). We also note that the position angle from

⁵ <https://gitlab.obspm.fr/gaia/nsstools>

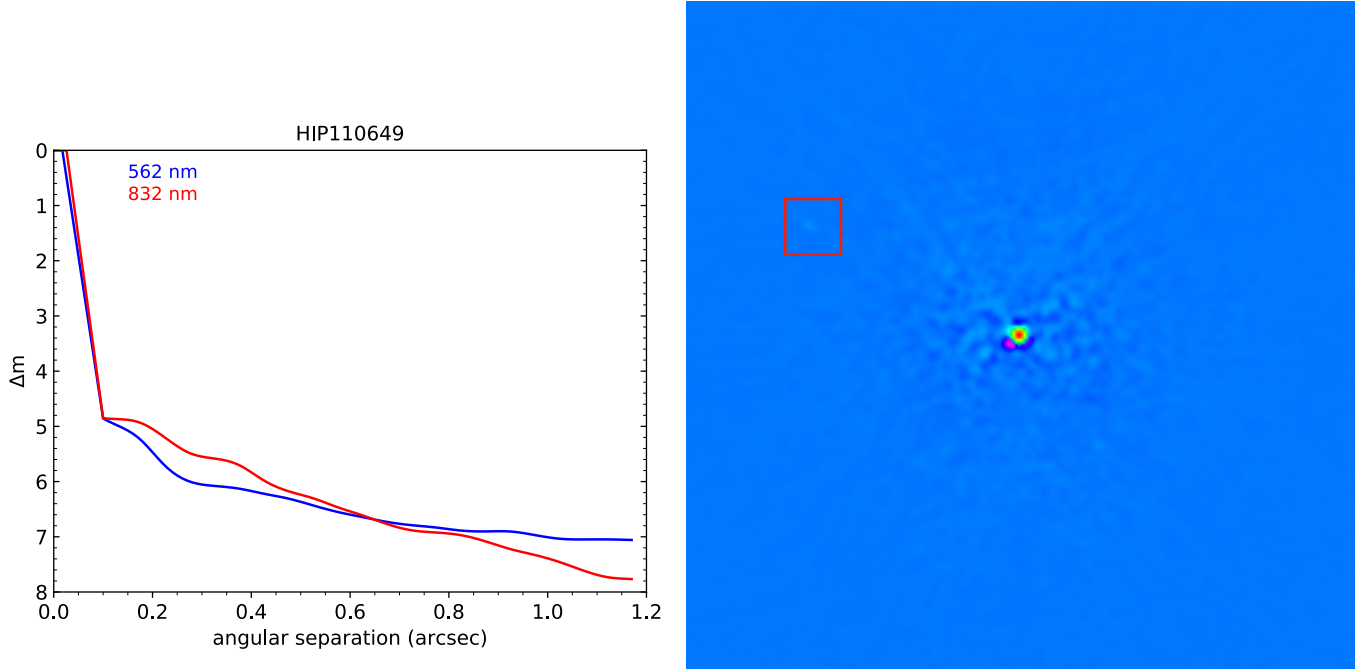


Figure 6. Left panel: Contrast curve from the 2020 Zorro Observations of HD 212330/TIC 259291108 from the ExoFOP archive. Right panel: Reconstructed image from the 832 nm filter. [Kane et al. \(2019\)](#) reported a companion at $0.77''$ with a position angle of 62° and a magnitude difference of 5.5 at 880 nm using DSSI on Gemini South in 2017. The red box highlights our possible detection of the same companion in this reconstructed image from 2020.

the Gaia orbit is not well-constrained, which could account for the remaining $\sim 80^\circ$ difference between our speckle measurement and the Gaia prediction. To calculate an error estimate for the position angle, we bootstrapped the orbital calculation 100,000 times with the orbital elements drawn from a Gaussian distribution based on the calculated orbital values and errors and taking the standard deviation of the resulting values. The error we derive on the Gaia position angle is $\sim 50^\circ$. While the position angles between the speckle and Gaia results are not in complete agreement, we believe our speckle detection and the Gaia companion are one in the same.

3.2. HD 212330/TIC 259291108

HD 212330 is a member of a known triple system. The star itself is G2 dwarf located ~ 20.3 pc away. A CPM companion at $23.957''$ is listed in the WDS and in [El-Badry et al. \(2021\)](#). A third inner component was identified in a combined radial velocity and speckle imaging study ([Kane et al. 2019](#)), which observed HD 212330 using DSSI on Gemini South on 2017, June 6. They found a companion at a separation of $\sim 0.77''$ with a magnitude difference of 6.7 at 692 nm and of 5.5 at 880 nm and a position angle of $\sim 62^\circ$. Five years later, [Tokovinin \(2023\)](#) observed the system using HRCam on the Southern Astrophysical Research telescope and resolved the companion at a separation of $0.8796''$, position angle of 244.6° and Δm of 5 mag in the I filter.

The star was also imaged in 2020 using Zorro on the Gemini South telescope. Figure 6 shows the Zorro observations of this target. The left panel shows the contrast curve and the right panel shows the reconstructed image from the 832 nm filter. The power spectrum from this observation shows no indication of a companion. However, looking at the right panel of Figure 6, there is a bright speckle at roughly the expected separation and position angle of the time-evolved companion from [Kane et al. \(2019\)](#). This is highlighted by the red square. Forcing a binary fit to the power spectrum yields a separation of $0.88''$ and a position angle of 63° , which is consistent with several of the orbit predictions. However, the fit yields a $\Delta m = 7.5$ compared to the ~ 5 found previously in the DSSI and HRCam observations.

To examine the discrepancy between the Zorro speckle observations and those from DSSI and HRCam, we fit a number of orbits for this system and predicted the corresponding positions of the companion at the time of the 2020 observations. The HRCam position angle was roughly 180° offset from the DSSI and Zorro observations likely due to the 180° ambiguity mentioned in Section 3.1, as the companion is quite faint. As such, we subtracted 180° from that

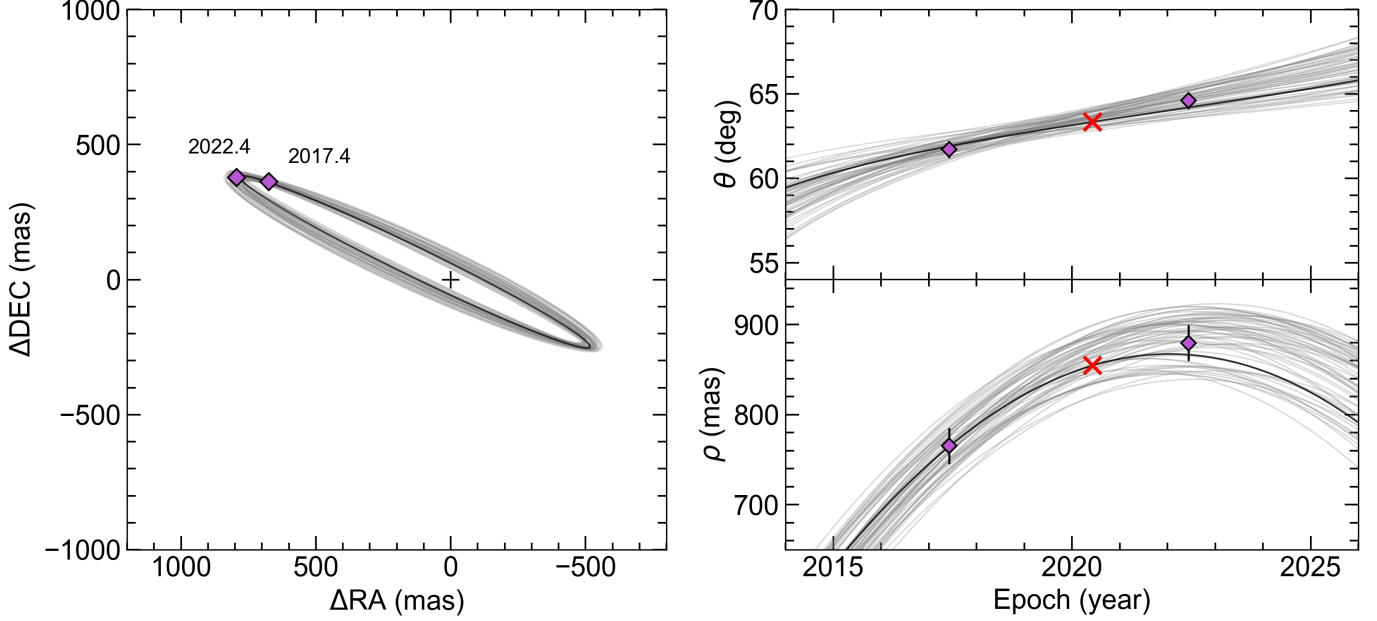


Figure 7. Orbit fit for HD 212330/TIC 259291108 using the astrometric data from [Kane et al. \(2019\)](#) at epoch 2017.4 and [Tokovinin \(2023\)](#) at epoch 2022.4, which are shown as purple diamonds, and the radial velocity fit from [Kane et al. \(2019\)](#). The black line represents the best fit, while the gray lines represent possible solutions within 2σ . The right panels show the separation and position angle of the orbit as a function of epoch. The \times symbol shows the predicted position of the stellar companion at the time of the 2020 Zorro observations, which is consistent with our fit to the data.

position angle to align with the other observations. For the orbit fit, we used Gaussian distributions for the period, epoch of periastron, eccentricity, and the longitude of periastron of the secondary star based on the the spectroscopic orbital solution from [Kane et al. \(2019\)](#). The inclination, angular semi-major axis, and longitude of the ascending node of the secondary star were free parameters with uniform distributions. We tested 10^7 combinations of these orbital parameters and calculated the χ^2 statistic of each solution. We removed all solutions with $\chi^2 > \chi^2_{\text{min}} + 10$. Our best-fit inclination was $85.55^\circ \pm 1.73^\circ$, our best-fit angular semi-major axis was $720.5 \text{ mas} \pm 23.7 \text{ mas}$, and our best-fit longitude of ascending node of the secondary was $244.1^\circ \pm 0.8^\circ$. Because of the 180° ambiguity in the [Tokovinin \(2023\)](#) results, the longitude also has an 180° ambiguity, meaning it could be $64.1^\circ \pm 0.8^\circ$. This would change the inclination to 94.45° . However, this would only change the orientation and direction of the orbit on-sky, not the physical properties of the system.

The visual orbits for these solutions and predicted positions of the companion at the time of the 2020 observation are plotted in Figure 7. Using the best-fit orbit, we predict the position of the companion during the 2020 Zorro observations. We find a predicted separation of $0.855''$ and a predicted position angle of 63.34° , which are consistent with the results from our fit to the data. As such, we find that this is the same stellar companion that was detected in the DSSI and HRCam observations, but at a much lower significance. This could explain why our Δm value is off from the other two observations. An examination of the night log finds that heavy clouds were present during the 2020 observations, which could explain the low significance.

3.3. Potential New Triple Systems

Six of the 27 targets found to be in multi-star systems are members of known triple systems: 11 LMi (TIC 8915802), σ^2 Eri (TIC 67772871), TW PsA (TIC 206686962), ϵ Ind (TIC 231698181), HD 212330 (TIC 259291108) and HD 90089 (TIC 367631379). Three of the 27 multiples are potentially new triple systems: 20 LMi (TIC 172954294), θ Per (TIC 302158903) and π^3 Ori (TIC 399665349).

20 LMi was listed by [Kirkpatrick et al. \(2024\)](#) as a triple due to its over-luminosity. However, the companion has not been observationally detected yet. While over-luminosity is a sign of multiplicity, it could also be caused by other factors, such as a star evolving from the main sequence. Because of this, we do not consider 20 LMi to be a triple system.

θ Per is a known multiple with a wide companion at $20.932''$ as noted in the WDS. [Tanner et al. \(2010\)](#) reported the potential detection of an additional brown dwarf companion that was unconfirmed in their study, but [Golovin et al. \(2023\)](#) lists only two components for this system. As such, we consider θ Per a binary rather than a triple system.

Finally, π^3 Ori currently has no confirmed companions. However, [Lafrenière et al. \(2007\)](#) notes that there were two point sources detected around π^3 Ori, but they did not obtain a second epoch of observation for this target. Furthermore, [González-Payo et al. \(2025\)](#), [Kirkpatrick et al. \(2024\)](#), and [Golovin et al. \(2023\)](#) consider this star to be single. As such, we consider this star single as well.

3.4. Assessing Potentially Missed Companions

One of the key goals of this study was to quantify the sensitivity of our existing speckle observations and determine what kinds of lower-mass stellar companions could remain undetected around these targets. To do this, we used a code developed to simulate possible stellar companions to our targets and assess our sensitivity to them ([Lund & Ciardi 2020](#); [Clark et al. 2022, 2024a,b](#)). We provide a brief description of the code below.

First, the mass, effective temperature, surface gravity and metallicity of the target star were retrieved from the TIC. For ten targets, the TIC did not have values or errors for one or more of the four parameters used. To correct this, we obtained these values from the ExEP target list, except for errors on the mass which were not given in the list. We took the average of the errors on the masses for the 70 other stars which had errors as an estimate for the errors on these values. In addition to this, six of the 80 stars were found to have directly measured masses listed by [Kirkpatrick et al. \(2024\)](#). We adopted those masses and errors on the mass for this analysis, with one exception. Taking these stellar parameters, a best-fit stellar isochrone was selected from the Dartmouth isochrones ([Dotter et al. 2008](#)). The errors on the masses are relatively large compared to the errors on the effective temperature and surface gravity, which can lead to a discrepancy between the input mass and the best-fit mass from the isochrone. However, all of our best-fit masses are within the input mass errors.

100,000 potential companions were then simulated following mass ratio and period distributions as described below. For our targets, we used two mass ratio and period distributions depending on the mass of the target. If the mass was between $0.6 M_\odot$ to $1.42 M_\odot$, we adopted the mass ratio and period distributions from [Raghavan et al. \(2010\)](#). We used the left panel of Figure 16 in [Raghavan et al. \(2010\)](#) to create a piecewise function where mass ratios in the intervals of 0-0.2, 0.2-0.95, and 0.95 - 1.0 have set values, and we normalized the resulting distribution. Below $0.6 M_\odot$, we used the distributions from [Duchêne & Kraus \(2013\)](#), who adopted a relatively flat power law distribution for the mass ratios and a normal distribution for the periods. In both cases, the minimum mass used for the simulations came from the best-fit isochrone and was roughly $0.1 M_\odot$ or spectral type M6. The minimum mass was divided by the mass of the target star to determine the minimum mass ratio used by the simulation. Beyond this minimum mass, there were no more points for the interpolation and, for our shown results, no companions with lower masses were simulated.

Figure 8 shows the results of this analysis for 71 Ori. The left panel shows Δm of the target star and the simulated companions as a function of physical separation. To determine this separation from our simulated period, we assumed circular orbits and use Kepler's Third law. We then randomized the location of the simulated companion within a sphere the size of the max separation and converted this back to a separation for use in the analysis. The red lines indicate where our speckle contrast curves fall on this plot. In some cases, we have multiple epochs of data for a target. All epochs are included in these plots and the best contrasts achieved overall are used. The contrast curves were then used to assess the sensitivity of each observation to these simulated companions. It is assumed that wide-field, seeing-limited imaging or Gaia would detect companions outside the field-of-view of the speckle instruments. The light blue shaded areas highlight the region where our speckle observations would not be sensitive to companions. As mentioned previously, our simulated companions only go to companions of spectral type M6 due to the isochrones being used. This is why there are no points below $\Delta m \sim 6.5$ in Figure 8. However, to test the potential effect of including lower mass companions, we extrapolated our interpolation to include masses down to $0.05 M_\odot$. We found a change of less than 2% when these systems are included. The percentage change is dependent on the mass of the primary star as this changes the mass-ratio distribution for the lowest mass targets in our sample.

The middle and right panels of Figure 8 show the period and mass ratio distributions for the simulated companions. The purple distribution represents all simulated companions, while the cyan distribution highlights those that would be undetected by our speckle observations. As seen, the majority of undetected companions are close-in systems and/or tend towards lower mass ratios.

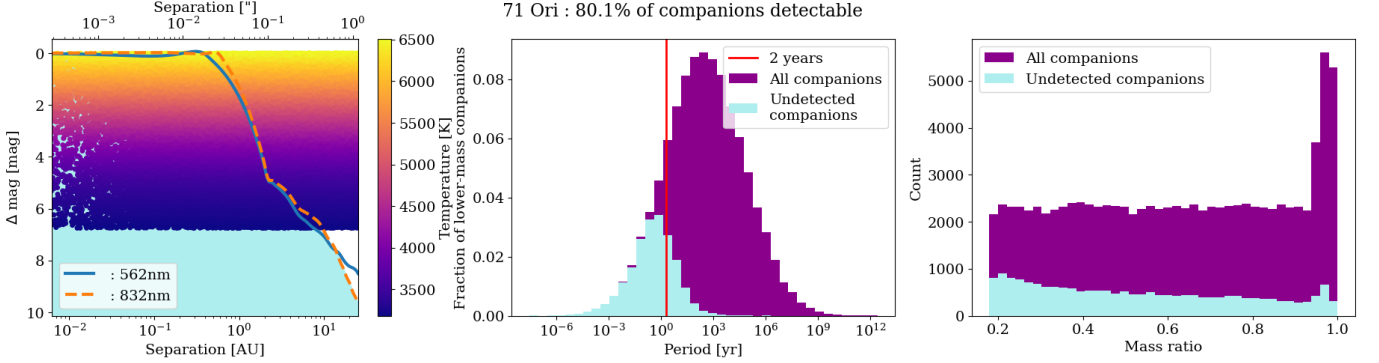


Figure 8. Results of the Missing Companions Analysis for 71 Ori. *Left:* Simulated stellar companions as a function of magnitude difference and separation. The color of the points indicates the effective temperatures of the simulated companions. The solid and dashed red lines show the contrast curves from our speckle observations. Above these lines, we would expect to detect the companion. The region of Δm vs. separation space that is shaded cyan represents the area where companions could reside and would not be detected by our speckle observations. The plot extends out to $1.17''$ as beyond this the correlation between the speckles breaks down and we lose detection sensitivity. For 71 Ori, this corresponds to a separation of 25.48 au. *Middle:* Period distributions of the simulated companions. The magenta histogram is the distribution of all 100,000 simulated companions, while the light blue histogram highlights what would not be detectable in our speckle observations. *Right:* Similar to the middle panel, but for mass ratio. We find that 80.1% of the simulated companions to this target are detected. Please see online Journal version for figures on the rest of the sample.

Overall, our simulations show that when speckle imaging is combined with wide-field imaging, $\sim 75\% - 85\%$ of simulated stellar companions should be detectable for our sample. This value depends on a number of factors, including the distance to the target star. Additionally, we treat each star as a single star for the purposes of assessing missing companions. A detected companion would decrease the area where a third component would exist. We do note that the code will eliminate some simulated stellar companions if those companions suggest existing planet orbits would fall within the Hill sphere of the companion. This is only done for target stars that have TOIs on ExoFOP. Among our 80 targets, only three are affected π^1 Men, HD 219134, and ρ^1 Cnc. In these cases, the planet's semi-major axes were calculated from the orbital period listed in the TOI catalog using Kepler's Third Law. The fact that our analysis only takes into account TOIs does bias our results for stars with planets detected through other methods. However, the magnitude of this bias depends on the location of the planet. For close-in planets, there may be no change in our detectable percentage as any removed binaries would be below our detection limits. Furthermore, we know that we are missing simulated companions below $0.1M_\odot$ which impacts the percentage detected. However, this change is relatively small, $< 2\%$ drop in the percentage of detectable companions.

4. DISCUSSION

4.1. Comparing 20-ms and 60-ms Observations

Currently, the recommended exposure time for ‘Alopeke and Zorro observations is 60-ms based on an analysis of bright stars. However, for many nearby, bright stars with $G < 5 - 7$ – which are prime targets for future space missions – this exposure time results in counts that are close to the saturation limits of ‘Alopeke and Zorro on the 8-m Gemini telescopes. This motivated the use of a 20-ms exposure time for our speckle observations of HWO targets. However, some of the stars in our sample have observations using both 60-ms and 20-ms exposure times, allowing us to compare and contrast.

We show four examples for HD 5015, HD 88230, β Com, and ζ^{02} Ret in Figure 9. For each star, we show the contrast curves obtained from both the 20-ms and 60-ms observations. In all four cases, no companion was detected. With the exception of HD 5015 and the November 2024 observation of HD 88230, the time spent on-target for the 20-ms observation was double what is normally spent on-target (six minutes instead of three). In all cases, the 20-ms and 60-ms observations produce similar results if no saturation occurs, with some slight improvements for observations which observed the target for longer.

4.2. Applications to Target Selection for HWO

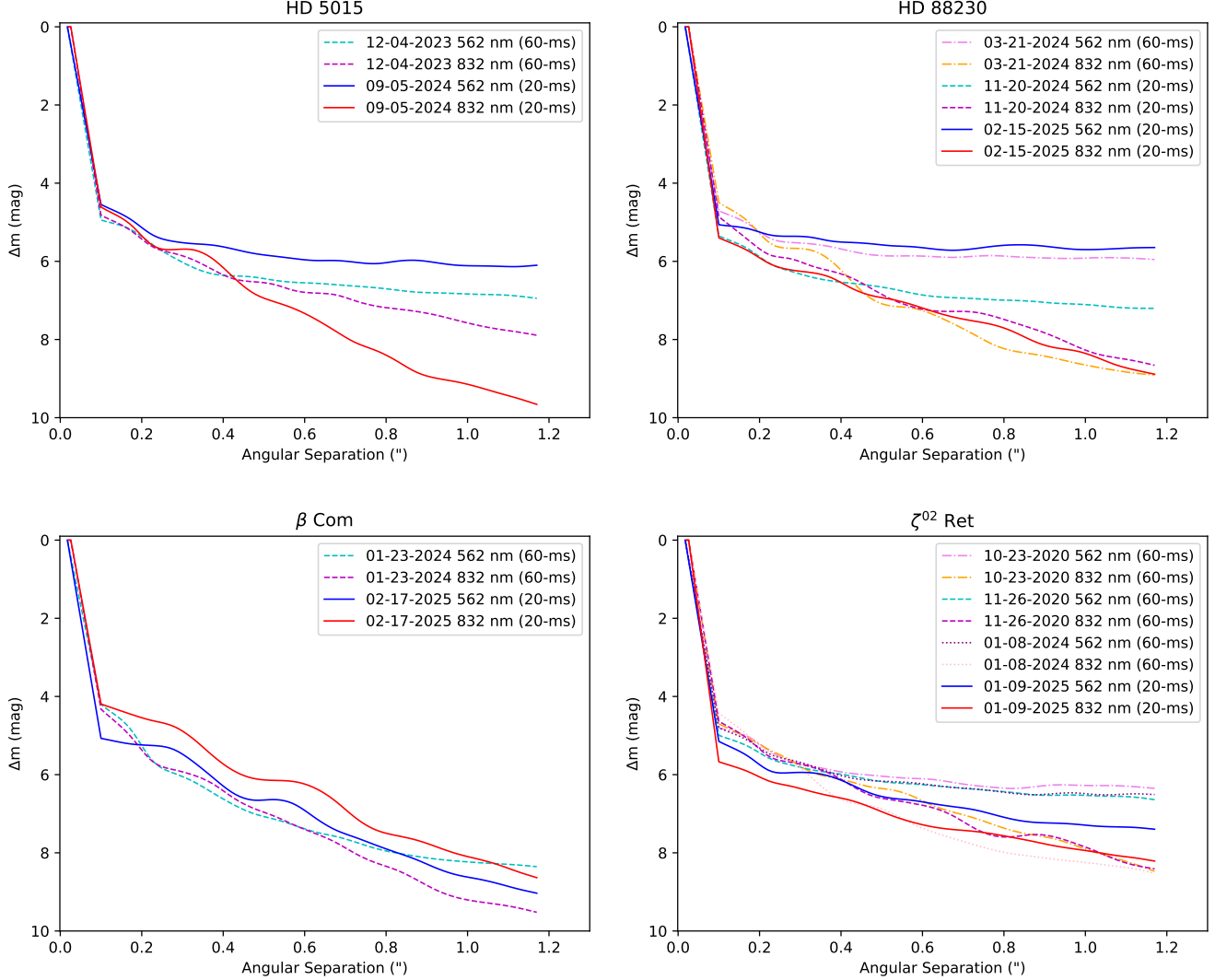


Figure 9. 20-ms and 60-ms contrast curves for HD 5015, HD 88230, β Com, and ζ^2 Ret. We find that similar results are produced for both exposure times.

Finding and characterizing stellar companions to potential HWO target stars is key to the success of the mission, both from a technical and a scientific perspective. As part of their effort to construct the ExEP provisional star list for HWO, Mamajek & Stapelfeldt (2024) consulted the WDS and the SB9 to remove close-in stellar companions with separations less than $3''$ that would likely interfere with HWO coronagraphic observations. Figure 5 shows that this effort was largely successful, as the majority of the companions identified in this work have separations larger than $3''$. However, our results also show that close-in stellar companions are still being identified around stars in this “cleaned” sample.

We have shown that Gaia can help in this effort. Its contributions include the identification of CPM companions at 100s to 1000s of arcseconds, as well as useful indicators to highlight stars that host a currently unresolved companion. In particular, the ability of Gaia to flag close-in companions as non-single stars enables targeted follow-up to confirm and assess the parameters of the companion. However, for the bright stars on the HWO target list, our results indicate that the Gaia indicators may not be reliable, in particular, the RUWE parameter (Figure 4). Therefore, caution needs to be exercised in using the RUWE values and other Gaia metrics to identify multiples amongst the brightest stars of the HWO target star list.

Overall, this work highlights the need for a uniform stellar multiplicity survey of all potential HWO targets using the best available facilities and a variety of techniques. Our missing companion analysis shows that, although speckle

imaging and wide field seeing limited imaging may detect the majority of companions, there is still the potential for a close-in or faint stellar companion around these target stars. To examine the region of separation and contrast space that these companions occupy, other methods such long-term spectroscopic observations, space-based techniques, or the use of high-resolution imaging on the Extremely Large Telescope needs to be utilized.

5. CONCLUSIONS

Much like the previous Great Observatories, the Habitable Worlds Observatory will be an enormous undertaking for the astronomical community. In order to ensure the success of one of its key missions, the direct-imaging of 25 habitable-zone exoplanets, we must thoroughly vet any star that may be on the final target list. This characterization includes an assessment of their abundances, ages, radii, masses, activity cycles, and nearby companions, both bound and unbound, stellar and planetary.

In this paper, we present results from new and archival speckle observations of 80 potential HWO targets stars drawn from the ExEP provisional star list for HWO (Mamajek & Stapelfeldt 2024). We present one new definitive detection, and an ambiguous detection of a known companion. After a search of Gaia and the literature, we find that 27 out of the 80 stars observed are in multi-star systems.

We note that 19 targets have elevated Gaia metrics indicating the potential presence of an unresolved companion. Two of these targets are flagged as NSS. However, we caution that bright targets may have higher astrometric errors than normal (Gaia Collaboration et al. 2023b), and as such, these Gaia indicators may not be as effective for bright targets. We find that only three of these 19 targets are shown to be multiples via other techniques. Two of those three are flagged as Gaia Non-single stars, with one confirmed by our speckle observations. The third target (TIC 259291108) has an elevated IPD_fmp value and is discuss in Section 3.2.

For each target that was observed with speckle imaging, we simulate potential stellar companions and assess our sensitivity to them using the contrast curves from our speckle observations. We find that the majority (75-85%) of simulated companions are recovered, although we caution that companions with masses lower than $\sim 0.1M_{\odot}$ are not included in this analysis. Furthermore, known companions and known planets other than TOIs are not included in the analysis. Future work will be to include these known stellar and substellar companions into the analysis. The undetected companions are very faint or very close-in. For these companions, we will need to implement long-term spectroscopic monitoring, use space-based techniques, or observe them using the high-angular resolution imagers that will be available on the ELTs.

We also find that 20-ms observations yield similar results to the typical 60-ms observations from ‘Alopeke and Zorro. This enables their use on bright targets that might prove difficult at other facilities.

Before the launch of HWO, many more potential targets will need to be vetted for stellar companions. By identifying which targets are part of multi-star systems and the parameters of the companions in those systems, we can enable the future architects of the final target list to make informed decisions on whether to include the examined stars as HWO targets. However, this work should to be started now rather than in five to ten years. This is because exoplanet yield simulations are being run now in order to help design and guide both the science design requirements and the optomechanical design of the mission. These simulations must be as realistic as possible and one of the key inputs into these simulations is the multiplicity of the potential target. High-resolution imaging, particularly speckle imaging, provides a time-efficient method for revealing companions at close separations and moderate contrasts. We are currently planning on observing the remainder of the ExEP list and more potential HWO targets with high resolution imaging as a next step in paving the road to the Habitable Worlds Observatory.

6. ACKNOWLEDGMENTS

We would like to thank the anonymous referee for their insightful comments. We would also like to thank Ruslan Belikov, Michael Bottom, Thierry Forveille, Madison LeBlanc, Tim Johns, and Dan Sirbu for their comments on a draft of this manuscript.

This research has made use of the Exoplanet Follow-up Observation Program (ExoFOP; DOI: 10.26134/ExoFOP5) website, which is operated by the California Institute of Technology, under contract with the National Aeronautics and Space Administration under the Exoplanet Exploration Program.

The International Gemini Observatory, a program of NSF NOIRLab, is managed by the Association of Universities for Research in Astronomy (AURA) under a cooperative agreement with the U.S. National Science Foundation on behalf of the Gemini partnership: the U.S. National Science Foundation (United States), the National Research Council

(Canada), Agencia Nacional de Investigación y Desarrollo (Chile), Ministerio de Ciencia, Tecnología e Innovación (Argentina), Ministério da Ciência, Tecnologia, Inovações e Comunicações (Brazil), and Korea Astronomy and Space Science Institute (Republic of Korea).

Observations in the paper made use of the High-Resolution Imaging instruments ‘Alopeke and Zorro. ‘Alopeke and Zorro were funded by the NASA Exoplanet Exploration Program and built at the NASA Ames Research Center by Steve B. Howell, Nic Scott, Elliott P. Horch, and Emmett Quigley. ‘Alopeke and Zorro were mounted on the Gemini North and South telescope of the international Gemini Observatory, a program of NSF NOIRLab, which is managed by the Association of Universities for Research in Astronomy (AURA) under a cooperative agreement with the U.S. National Science Foundation. on behalf of the Gemini partnership: the U.S. National Science Foundation (United States), National Research Council (Canada), Agencia Nacional de Investigación y Desarrollo (Chile), Ministerio de Ciencia, Tecnología e Innovación (Argentina), Ministério da Ciência, Tecnologia, Inovações e Comunicações (Brazil), and Korea Astronomy and Space Science Institute (Republic of Korea).

Based on observations at NSF Kitt Peak National Observatory, NSF NOIRLab (Prop:2017A-0006, 2023A-807455 PI: S.B. Howell), which is managed by the Association of Universities for Research in Astronomy (AURA) under a cooperative agreement with the U.S. National Science Foundation. The authors are honored to be permitted to conduct astronomical research on I’oligam Du’ag (Kitt Peak), a mountain with particular significance to the Tohono O’odham.

Some of the observations in the paper made use of the NN-EXPLORE Exoplanet and Stellar Speckle Imager (NESSI). NESSI was funded by the NASA Exoplanet Exploration Program and the NASA Ames Research Center. NESSI was built at the Ames Research Center by Steve B. Howell, Nic Scott, Elliott P. Horch, and Emmett Quigley.

This research has made use of the Washington Double Star Catalog maintained at the U.S. Naval Observatory.

We acknowledge financial support from the Agencia Estatal de Investigación (AEI/10.13039/501100011033) of the Ministerio de Ciencia e Innovación and the ERDF “A way of making Europe” through project PID2022-137241NB-C42.

Part of this research was carried out at the Jet Propulsion Laboratory, California Institute of Technology, under a contract with the National Aeronautics and Space Administration (80NM0018D0004).

REFERENCES

Baroch, D., Morales, J. C., Ribas, I., et al. 2018, *A&A*, 619, A32, doi: [10.1051/0004-6361/201833440](https://doi.org/10.1051/0004-6361/201833440)

Belikov, R., Bendek, E., Thomas, S., Males, J., & Lozi, J. 2015, in Society of Photo-Optical Instrumentation Engineers (SPIE) Conference Series, Vol. 9605, Techniques and Instrumentation for Detection of Exoplanets VII, ed. S. Shaklan, 960517, doi: [10.1117/12.2188732](https://doi.org/10.1117/12.2188732)

Bendek, E. A., Belikov, R., Sirbu, D., et al. 2021, in Society of Photo-Optical Instrumentation Engineers (SPIE) Conference Series, Vol. 11823, Techniques and Instrumentation for Detection of Exoplanets X, ed. S. B. Shaklan & G. J. Ruane, 1182311, doi: [10.1117/12.2594992](https://doi.org/10.1117/12.2594992)

Bohn, A. J., Southworth, J., Ginski, C., et al. 2020, *A&A*, 635, A73, doi: [10.1051/0004-6361/201937127](https://doi.org/10.1051/0004-6361/201937127)

Cifuentes, C., Caballero, J. A., González-Payo, J., et al. 2025, *A&A*, 693, A228, doi: [10.1051/0004-6361/202452527](https://doi.org/10.1051/0004-6361/202452527)

Clark, C. A., van Belle, G. T., Ciardi, D. R., et al. 2022, *AJ*, 163, 232, doi: [10.3847/1538-3881/ac6101](https://doi.org/10.3847/1538-3881/ac6101)

Clark, C. A., van Belle, G. T., Horch, E. P., et al. 2024a, *AJ*, 167, 56, doi: [10.3847/1538-3881/ad0bfd](https://doi.org/10.3847/1538-3881/ad0bfd)

—. 2024b, *AJ*, 167, 174, doi: [10.3847/1538-3881/ad267d](https://doi.org/10.3847/1538-3881/ad267d)

Dotter, A., Chaboyer, B., Jevremović, D., et al. 2008, *ApJS*, 178, 89, doi: [10.1086/589654](https://doi.org/10.1086/589654)

Duchêne, G., & Kraus, A. 2013, *ARA&A*, 51, 269, doi: [10.1146/annurev-astro-081710-102602](https://doi.org/10.1146/annurev-astro-081710-102602)

Duquennoy, A., & Mayor, M. 1991, *A&A*, 248, 485

El-Badry, K., Rix, H.-W., & Heintz, T. M. 2021, *MNRAS*, 506, 2269, doi: [10.1093/mnras/stab323](https://doi.org/10.1093/mnras/stab323)

Feng, F., Butler, R. P., Vogt, S. S., et al. 2022, *ApJS*, 262, 21, doi: [10.3847/1538-4365/ac7e57](https://doi.org/10.3847/1538-4365/ac7e57)

Gaia Collaboration, Prusti, T., de Bruijne, J. H. J., et al. 2016, *A&A*, 595, A1, doi: [10.1051/0004-6361/201629272](https://doi.org/10.1051/0004-6361/201629272)

Gaia Collaboration, Smart, R. L., Sarro, L. M., et al. 2021a, *A&A*, 649, A6, doi: [10.1051/0004-6361/202039498](https://doi.org/10.1051/0004-6361/202039498)

Gaia Collaboration, Brown, A. G. A., Vallenari, A., et al. 2021b, *A&A*, 649, A1, doi: [10.1051/0004-6361/202039657](https://doi.org/10.1051/0004-6361/202039657)

Gaia Collaboration, Arenou, F., Babusiaux, C., et al. 2023a, *A&A*, 674, A34, doi: [10.1051/0004-6361/202243782](https://doi.org/10.1051/0004-6361/202243782)

Gaia Collaboration, Vallenari, A., Brown, A. G. A., et al. 2023b, *A&A*, 674, A1, doi: [10.1051/0004-6361/202243940](https://doi.org/10.1051/0004-6361/202243940)

Gatewood, G., & Gatewood, C. 2016, *Journal of Double Star Observations*, 12, 580

Golovin, A., Reffert, S., Just, A., et al. 2023, *A&A*, 670, A19, doi: [10.1051/0004-6361/202244250](https://doi.org/10.1051/0004-6361/202244250)

González-Payo, J., Caballero, J. A., Gorgas, J., et al. 2024, *A&A*, 689, A302, doi: [10.1051/0004-6361/202450048](https://doi.org/10.1051/0004-6361/202450048)

González-Payo, J., Caballero, J. A., Cifuentes, C., et al. 2025, *A&A*, Submitted

Haghighipour, N., & Raymond, S. N. 2007, *ApJ*, 666, 436, doi: [10.1086/520501](https://doi.org/10.1086/520501)

Halbwachs, J.-L., Pourbaix, D., Arenou, F., et al. 2023, *A&A*, 674, A9, doi: [10.1051/0004-6361/202243969](https://doi.org/10.1051/0004-6361/202243969)

Hamers, A. S., Rantala, A., Neunteufel, P., Preece, H., & Vynatheya, P. 2021, *MNRAS*, 502, 4479, doi: [10.1093/mnras/stab287](https://doi.org/10.1093/mnras/stab287)

Hartkopf, W. I., Mason, B. D., & Worley, C. E. 2001, *AJ*, 122, 3472, doi: [10.1086/323921](https://doi.org/10.1086/323921)

Hawkins, K., Lucey, M., Ting, Y.-S., et al. 2020, *MNRAS*, 492, 1164, doi: [10.1093/mnras/stz3132](https://doi.org/10.1093/mnras/stz3132)

Heintz, T. M., Hermes, J. J., Tremblay, P. E., et al. 2024, *ApJ*, 969, 68, doi: [10.3847/1538-4357/ad479b](https://doi.org/10.3847/1538-4357/ad479b)

Hirsch, L. A., Rosenthal, L., Fulton, B. J., et al. 2021, *AJ*, 161, 134, doi: [10.3847/1538-3881/abd639](https://doi.org/10.3847/1538-3881/abd639)

Horch, E. P., Gomez, S. C., Sherry, W. H., et al. 2011a, *AJ*, 141, 45, doi: [10.1088/0004-6256/141/2/45](https://doi.org/10.1088/0004-6256/141/2/45)

Horch, E. P., van Altena, W. F., Howell, S. B., Sherry, W. H., & Ciardi, D. R. 2011b, *AJ*, 141, 180, doi: [10.1088/0004-6256/141/6/180](https://doi.org/10.1088/0004-6256/141/6/180)

Horch, E. P., Veillette, D. R., Baena Gallé, R., et al. 2009, *AJ*, 137, 5057, doi: [10.1088/0004-6256/137/6/5057](https://doi.org/10.1088/0004-6256/137/6/5057)

Howell, S. B., Everett, M. E., Sherry, W., Horch, E., & Ciardi, D. R. 2011, *AJ*, 142, 19, doi: [10.1088/0004-6256/142/1/19](https://doi.org/10.1088/0004-6256/142/1/19)

Hutter, D. J., Tycner, C., Zavala, R. T., et al. 2019, *ApJS*, 243, 32, doi: [10.3847/1538-4365/ab32e1](https://doi.org/10.3847/1538-4365/ab32e1)

Jang-Condell, H. 2015, *ApJ*, 799, 147, doi: [10.1088/0004-637X/799/2/147](https://doi.org/10.1088/0004-637X/799/2/147)

Kane, S. R., Dalba, P. A., Li, Z., et al. 2019, *AJ*, 157, 252, doi: [10.3847/1538-3881/ab1ddf](https://doi.org/10.3847/1538-3881/ab1ddf)

Kirkpatrick, J. D., Marocco, F., Gelino, C. R., et al. 2024, *ApJS*, 271, 55, doi: [10.3847/1538-4365/ad24e2](https://doi.org/10.3847/1538-4365/ad24e2)

Kraus, A. L., Ireland, M. J., Huber, D., Mann, A. W., & Dupuy, T. J. 2016, *AJ*, 152, 8, doi: [10.3847/0004-6256/152/1/8](https://doi.org/10.3847/0004-6256/152/1/8)

Lafrenière, D., Doyon, R., Marois, C., et al. 2007, *ApJ*, 670, 1367, doi: [10.1086/522826](https://doi.org/10.1086/522826)

Lester, K. V., Matson, R. A., Howell, S. B., et al. 2021, *AJ*, 162, 75, doi: [10.3847/1538-3881/ac0d06](https://doi.org/10.3847/1538-3881/ac0d06)

Lohmann, A. W., Weigelt, G., & Wirnitzer, B. 1983, *ApOpt*, 22, 4028, doi: [10.1364/AO.22.004028](https://doi.org/10.1364/AO.22.004028)

Lund, M. B., & Ciardi, D. 2020, in American Astronomical Society Meeting Abstracts, Vol. 235, American Astronomical Society Meeting Abstracts #235, 249.06

Mamajek, E., & Stapelfeldt, K. 2024, arXiv e-prints, arXiv:2402.12414, doi: [10.48550/arXiv.2402.12414](https://doi.org/10.48550/arXiv.2402.12414)

Mason, B. D., Wycoff, G. L., Hartkopf, W. I., Douglass, G. G., & Worley, C. E. 2001, *AJ*, 122, 3466, doi: [10.1086/323920](https://doi.org/10.1086/323920)

Matson, R. A., Howell, S. B., & Ciardi, D. R. 2019, *AJ*, 157, 211, doi: [10.3847/1538-3881/ab1755](https://doi.org/10.3847/1538-3881/ab1755)

Matson, R. A., Gore, R., Howell, S. B., et al. 2025, *AJ*, 169, 76, doi: [10.3847/1538-3881/ad9923](https://doi.org/10.3847/1538-3881/ad9923)

McAlister, H. A., Hartkopf, W. I., Sowell, J. R., Dombrowski, E. G., & Franz, O. G. 1989, *AJ*, 97, 510, doi: [10.1086/115001](https://doi.org/10.1086/115001)

Moe, M., & Kratter, K. M. 2021, *MNRAS*, 507, 3593, doi: [10.1093/mnras/stab2328](https://doi.org/10.1093/mnras/stab2328)

of Sciences Engineering, N. A., & Medicine. 2021, *Pathways to Discovery in Astronomy and Astrophysics for the 2020s* (Washington D.C.: National Academies Press)

Offner, S. S. R., Moe, M., Kratter, K. M., et al. 2023, in *Astronomical Society of the Pacific Conference Series*, Vol. 534, *Protostars and Planets VII*, ed. S. Inutsuka, Y. Aikawa, T. Muto, K. Tomida, & M. Tamura, 275, doi: [10.48550/arXiv.2203.10066](https://doi.org/10.48550/arXiv.2203.10066)

Paegert, M., Stassun, K. G., Collins, K. A., et al. 2021, arXiv e-prints, arXiv:2108.04778, doi: [10.48550/arXiv.2108.04778](https://doi.org/10.48550/arXiv.2108.04778)

Pourbaix, D., Tokovinin, A. A., Batten, A. H., et al. 2004, *A&A*, 424, 727, doi: [10.1051/0004-6361:20041213](https://doi.org/10.1051/0004-6361:20041213)

Quintana, E. V., & Lissauer, J. J. 2006, *Icarus*, 185, 1, doi: [10.1016/j.icarus.2006.06.016](https://doi.org/10.1016/j.icarus.2006.06.016)

Rafikov, R. R., & Silsbee, K. 2015a, *ApJ*, 798, 69, doi: [10.1088/0004-637X/798/2/69](https://doi.org/10.1088/0004-637X/798/2/69)

—. 2015b, *ApJ*, 798, 70, doi: [10.1088/0004-637X/798/2/70](https://doi.org/10.1088/0004-637X/798/2/70)

Raghavan, D., McAlister, H. A., Henry, T. J., et al. 2010, *ApJS*, 190, 1, doi: [10.1088/0067-0049/190/1/1](https://doi.org/10.1088/0067-0049/190/1/1)

Scott, N. J., & Howell, S. B. 2018, in *Society of Photo-Optical Instrumentation Engineers (SPIE) Conference Series*, Vol. 10701, *Optical and Infrared Interferometry and Imaging VI*, ed. M. J. Creech-Eakman, P. G. Tuthill, & A. Mérand, 107010G, doi: [10.1117/12.2311539](https://doi.org/10.1117/12.2311539)

Scott, N. J., Howell, S. B., Gnilka, C. L., et al. 2021, *Frontiers in Astronomy and Space Sciences*, 8, 138, doi: [10.3389/fspas.2021.716560](https://doi.org/10.3389/fspas.2021.716560)

Scowen, P., Bolcar, M., & Zhao, F. 2025, in *American Astronomical Society Meeting Abstracts*, Vol. 245, *American Astronomical Society Meeting Abstracts*, 305.04

Sirbu, D., Belikov, R., Bendek, E., et al. 2023, in Society of Photo-Optical Instrumentation Engineers (SPIE) Conference Series, Vol. 12680, Society of Photo-Optical Instrumentation Engineers (SPIE) Conference Series, 126800Y, doi: [10.1117/12.2677778](https://doi.org/10.1117/12.2677778)

Sirbu, D., Thomas, S., Belikov, R., & Bendek, E. 2017, *ApJ*, 849, 142, doi: [10.3847/1538-4357/aa8e02](https://doi.org/10.3847/1538-4357/aa8e02)

Stassun, K. G., Oelkers, R. J., Paegert, M., et al. 2019, *AJ*, 158, 138, doi: [10.3847/1538-3881/ab3467](https://doi.org/10.3847/1538-3881/ab3467)

Sullivan, K., Kraus, A. L., Berger, T. A., et al. 2024, *AJ*, 168, 129, doi: [10.3847/1538-3881/ad6310](https://doi.org/10.3847/1538-3881/ad6310)

Tanner, A. M., Gelino, C. R., & Law, N. M. 2010, *PASP*, 122, 1195, doi: [10.1086/656481](https://doi.org/10.1086/656481)

Teske, J. K., Everett, M. E., Hirsch, L., et al. 2015, *AJ*, 150, 144, doi: [10.1088/0004-6256/150/5/144](https://doi.org/10.1088/0004-6256/150/5/144)

Thebault, P., & Haghighipour, N. 2015, in *Planetary Exploration and Science: Recent Results and Advances*, ed. S. Jin, N. Haghighipour, & W.-H. Ip (Springer), 309–340, doi: [10.1007/978-3-662-45052-9_13](https://doi.org/10.1007/978-3-662-45052-9_13)

Thomas, S., Belikov, R., & Bendek, E. 2015, *ApJ*, 810, 81, doi: [10.1088/0004-637X/810/1/81](https://doi.org/10.1088/0004-637X/810/1/81)

Tokovinin, A. 2014, *AJ*, 147, 87, doi: [10.1088/0004-6256/147/4/87](https://doi.org/10.1088/0004-6256/147/4/87)

—. 2017, *MNRAS*, 468, 3461, doi: [10.1093/mnras/stx707](https://doi.org/10.1093/mnras/stx707)

—. 2023, *AJ*, 165, 180, doi: [10.3847/1538-3881/acc464](https://doi.org/10.3847/1538-3881/acc464)

Ward-Duong, K., Patience, J., De Rosa, R. J., et al. 2015, *MNRAS*, 449, 2618, doi: [10.1093/mnras/stv384](https://doi.org/10.1093/mnras/stv384)

Zucker, S., Mazeh, T., Santos, N. C., Udry, S., & Mayor, M. 2004, *A&A*, 426, 695, doi: [10.1051/0004-6361:20040384](https://doi.org/10.1051/0004-6361:20040384)

Table 1. Potential HWO Target Stars Observed

TIC ID	Gaia DR3 ID	Simbad Name	R.A.	decl.	$PM_{R.A.}$	$PM_{decl.}$	π	G	$G - G_{RP}$
-	-	-	[$^{\circ}$]	[$^{\circ}$]	[mas/yr]	[mas/yr]	[mas]	[mag]	[mag]
3962869	2473608009504466688	ϕ^2 Cet	12.53059	-10.64535	-228.03115	-229.5775	0.0628	5.02954	0.41624
8915802	798068905726303232	11 LMi	143.91061	35.80898	-726.51388	-259.05745	0.08901	5.20043	0.54685
11310083	5663558453071724288	HD 84117	145.55813	-23.9144	-399.49675	262.31931	0.06688	4.77215	0.419
21535479	777254360337133312	47 UMa	164.8647	40.4305	-316.8499	55.1804	0.07201	4.86659	0.47652
23969522	821455861647126656	15 LMi	147.1488	46.0206	221.75005	-92.35563	0.05313	4.91655	0.46953
27136704	3407611182744289152	μ Tau	76.86503	18.64513	534.67392	18.44878	0.06283	4.73246	0.49986
38511251	5164120762333028736	δ Eri	55.81166	-9.76008	-93.63406	744.36039	0.11003	3.27557	0.5888
46125330	3374052988354372992	71 Ori	93.71153	19.15564	-97.60836	-182.44758	0.04592	5.07295	0.35995
47346402	3400292798990117888	111 Tau	81.10726	17.3835	250.4829	-7.15628	0.06859	4.85019	0.42812
60716322	2719475542667772416	ξ Peg	341.67431	12.17069	233.35408	-493.13255	0.06092	4.06936	0.4435
67772871	3195919528989223040	σ^2 Eri	63.80795	-7.66808	-2240.08498	-3421.80862	0.19961	4.17989	0.61014
72748794	5117974602912370432	HD 14412	34.74269	-25.94371	-217.73411	444.60889	0.07791	6.14786	0.5497
80226651	3381727613874753536	37 Gem	103.82759	25.3758	-37.59497	24.23372	0.05746	5.60278	0.47347
95431211	624684408880100992	40 Leo	154.93294	19.46996	-230.58856	-214.06859	0.04713	4.65715	0.37559
101641846	4025850731201819392	61 UMa	175.2625	34.19994	-12.52161	-381.19587	0.10443	5.111	0.52984
113710966	96331172942614528	107 Psc	25.62259	20.26552	-300.73692	-673.5389	0.13082	4.99968	0.58235
116988032	436648129327098496	ι Per	47.2754	49.61287	1262.19279	-91.08282	0.09454	3.90264	0.47579
117979951	2980492387558410112	58 Eri	71.90182	-16.9337	130.26356	169.33843	0.07553	5.31838	0.4909
118572803	5164707970261890560	ϵ Eri	53.22829	-9.45817	-974.75815	20.87584	0.31058	3.46575	0.6236
135656809	4345775217221821312	18 Sco	243.90634	-8.37164	232.23032	-495.3782	0.07074	5.32765	0.4898
141810080	5264749303462961280	α Men	92.56236	-74.75399	121.59582	-212.41088	0.09792	4.90014	0.53205
147407292	6564091190988411520	HD 207129	327.06671	-47.30493	165.06854	-295.55273	0.06427	5.41939	0.47192
155315739	6553614253923452800	HD 217987	346.50392	-35.84716	6765.99514	1330.28527	0.30414	6.52203	1.03053
156890613	974887555341533440	HD 55575	108.95911	47.23914	30.07864	-185.90471	0.05934	5.38816	0.47489
157364190	1384195086792268800	χ Her	238.17156	42.45432	438.83869	629.54062	0.0629	4.42426	0.46506
157966796	1284257623084916480	σ Boo	218.67104	29.74571	188.57436	131.57967	0.06347	4.34196	0.33059
165602000	1872046609345556480	61 Cyg A	316.74848	38.76386	4164.20869	3249.61388	0.28599	4.76671	0.78951
165602023	1872046574983497216	61 Cyg B	316.75366	38.75607	4105.97643	3155.94164	0.28601	5.45064	0.89373
166646191	762815470562110464	HD 95735	165.83096	35.94865	-580.05709	-4776.58872	0.39275	6.55117	1.07566
172954294	746545172372256384	20 LMi	150.24997	31.92176	-528.87061	-429.37566	0.067	5.20496	0.50104
176521059	3023711269067191296	HD 38858	87.14586	-4.09566	61.427	-229.2912	0.06574	5.80588	0.49249
179348425	6009538585839374336	HD 140901	236.86891	-37.91726	-415.50658	-213.99094	0.06559	5.83384	0.52322
189576919	348020482735930112	υ And	24.19832	41.40376	-171.89184	-381.81516	0.07419	3.96613	0.45044
202380743	16611568850770761600	HD 122064	209.38328	61.49382	-31.69308	216.28964	0.09933	6.16992	0.68668
206686962	6604147121141267712	TW PsA	344.10194	-31.56627	330.20338	-158.60233	0.13155	6.09186	0.74553
213041474	3211461469444773376	HD 32147	75.20662	-5.7586	549.30869	-1108.24503	0.11307	5.88649	0.6996
219709102	1068982214258617216	σ^2 UMa	137.59826	67.13363	13.1189	-87.88146	0.04874	4.67962	0.39739
229092427	4934923028038871296	ν Phe	18.80056	-45.53087	665.08565	178.0698	0.06553	4.82792	0.44801
229902025	1264630412816366720	c Boo	226.82618	24.86846	184.71405	-164.27907	0.05119	4.8023	0.36277
231698181	6412595290592307840	ϵ Ind	330.87241	-56.79725	3966.66054	-2536.19199	0.27484	4.3229	0.71235
238432056	2860924621205256704	HD 166	1.6552	29.02071	380.15925	-177.7296	0.07264	5.87833	0.54521
257393898	2552925644460225152	HD 4628	12.09911	5.27554	755.8935	-1141.7193	0.13449	5.46769	0.63892
259237827	2261614264931057664	σ Dra	293.0976	69.65345	597.38424	-1738.2861	0.17349	4.44904	0.58387
259291108	6408551802222368384	HD 212330	336.23595	-57.79902	129.65788	-352.4248	0.04916	5.15285	0.52138
261136679	4623036865373793408	π Men	84.29954	-80.46446	310.90883	1049.06049	0.05468	5.51158	0.46077
279649049	4722135642226902656	ζ^2 Ret	49.56623	-62.50348	1331.02709	647.7254	0.08306	5.07961	0.48554
279649057	4722111590409480064	ζ^1 Ret	49.45525	-62.57243	1337.53038	649.83975	0.08302	5.34462	0.50483
283722336	2009481748875806976	HD 219134	348.33773	57.16967	2074.41351	294.45198	0.15286	5.2319	0.68166
285544488	427322415301550208	HD 5015	13.26686	61.12473	-68.29788	169.43506	0.0529	4.63591	0.43715
289673491	2416611663182821120	6 Cet	2.81569	-15.46918	-82.82753	-269.54932	0.05295	4.76362	0.42554

Table 1 *continued on next page*

Table 1 (*continued*)

TIC ID	Gaia DR3 ID	Simbad Name	R.A.	decl.	$PM_{R.A.}$	$PM_{decl.}$	π	G	$G - G_{RP}$
-	-	-	[$^{\circ}$]	[$^{\circ}$]	[mas/yr]	[mas/yr]	[mas]	[mag]	[mag]
301051051	4847957293278177024	e Eri	50.00034	-43.06655	3035.01732	726.96448	0.16552	4.06392	0.55562
302158903	438829629114680704	θ Per	41.05222	49.22805	334.70816	-89.25073	0.08968	3.983	0.42831
309599261	4034171629042489088	HD 103095	178.26735	37.69283	4002.65464	-5817.80019	0.10903	6.1985	0.59273
311063391	263916708025623680	HD 37394	85.33475	53.47873	2.80354	-523.47749	0.0815	5.99095	0.58834
311092847	3263836568394170880	10 Tau	54.21723	0.39952	-232.56337	-481.47228	0.07184	4.14109	0.46525
328324648	976893923544104576	22 Lyn	112.48392	49.67209	111.04698	-82.88428	0.04901	5.22393	0.39558
332064670	704967037090946688	ρ^1 Cnc	133.14676	28.32978	-485.68081	-233.51701	0.07945	5.73268	0.58567
343813545	3269362645115584640	κ^1 Cet	49.8416	3.37062	269.29794	93.95652	0.1078	4.65649	0.50198
355127594	714116137767540096	HD 78366	137.21177	33.88171	-191.41313	-114.6302	0.05277	5.80906	0.46222
366661076	3796442680948579328	β Vir	177.67712	1.76352	740.74634	-270.92723	0.09089	3.46856	0.46228
367631379	1146337324038514176	HD 90089	157.76666	82.55874	-86.13273	19.83218	0.04344	5.14406	0.34225
371520835	823773494718931968	HD 88230	152.83293	49.45199	-1363.28719	-505.77036	0.20531	5.96117	0.89508
373694425	512167948043650816	HD 10780	26.94268	63.85141	581.68397	-246.46227	0.09959	5.4104	0.56842
373765355	3936909723803146368	HD 115404	199.21567	17.016	636.28474	-264.67829	0.09102	6.29768	0.63509
377415363	1193030490492925824	γ Ser	239.1147	15.65591	311.18255	-1282.76704	0.08956	3.69443	0.40156
389853353	1521686782461765888	10 CVn	191.24546	39.27953	-359.69875	139.0162	0.05696	5.80303	0.46462
399665349	3288921720025503360	π^3 Ori	72.46212	6.96133	463.9544	11.93701	0.12462	3.08792	0.37977
409104974	188771135583573504	λ Aur	79.78834	40.0961	520.56891	-664.48787	0.0796	4.52588	0.46843
416519065	853819947756949120	36 UMa	157.65517	55.98039	-177.0448	-32.63371	0.07725	4.67389	0.42207
417762326	1092545710514654464	π^1 UMa	129.79848	65.0213	-27.27447	87.88083	0.06926	5.49898	0.48628
419015728	2452378776434477184	τ Cet	26.00906	-15.93368	-1721.72779	854.96316	0.27381	3.3004	0.5521
425935521	4900108950849461248	ζ Tuc	5.03561	-64.86962	1706.74686	1164.95944	0.11618	4.07351	0.47331
434210589	2802397960855105920	54 Psc	9.83865	21.24883	-461.94829	-369.62427	0.09002	5.65432	0.59171
437886584	3331979901042416512	k Ori	94.11129	12.27299	82.77515	186.48042	0.05105	4.91641	0.36162
441709021	1604859511344724864	θ Boo	216.29746	51.84897	-235.96992	-399.6957	0.06907	3.91723	0.43786
445070560	1460229442589223424	β Com	197.96428	27.88211	-800.7201	882.30132	0.10873	4.09328	0.46766
445258206	425040000962559616	η Cas	12.28523	57.81273	1078.60917	-551.13342	0.16883	3.32007	0.47145
458445966	1534011998572555776	β CVn	188.43143	41.35878	-704.70212	292.15466	0.11803	4.09467	0.49284
1101124558	1237090738916392704	ξ Boo	222.84805	19.10027	127.46788	-40.56865	0.14807	4.48048	0.53605
1101124559	1237090738916392832	ξ Boo B	222.84664	19.1011	133.37605	-182.05918	0.14818	6.43009	0.81497

NOTE—Coordinates are on ICRS frame and in epoch 2016.0.

Table 2. Speckle Imaging Results

TIC ID	Instrument	P.I.	Date	562 nm		832 nm	
				Contrast @ 0.1''	Contrast @ 0.5''	Contrast @ 0.1''	Contrast @ 0.5''
-	-	-	yyyy/mm/dd	[mag]	[mag]	[mag]	[mag]
3962869	'Alopeke	Burt	2020/08/10	5.280	6.755	4.951	7.131
8915802	'Alopeke	Hartman	2025/02/18	5.034	7.588	5.142	7.136
11310083	Zorro	Howell	2020/12/31	5.395	6.609	5.234	6.677
21535479	'Alopeke	Hartman	2025/02/17	4.803	6.090	4.360	6.874
23969522	'Alopeke	Hartman	2025/02/17	4.888	7.014	4.070	6.835
27136704	'Alopeke	Hartman	2024/09/26	4.818	7.159	3.862	6.856
"	"	"	2025/02/18	5.219	7.093	4.622	6.799
38511251	'Alopeke	Burt	2020/12/06	4.729	5.619	4.949	6.883
46125330	'Alopeke	Hartman	2025/02/16	4.886	7.231	4.830	7.092
47346402	'Alopeke	Hartman	2025/02/18	5.059	7.019	4.121	7.025
60716322	'Alopeke	Burt	2024/05/25	4.650	6.665	4.545	6.850
67772871	'Alopeke	Burt	2020/12/06	5.034	6.480	4.516	6.757
72748794	'Alopeke	Burt	2020/11/24	5.474	7.159	4.763	6.443
80226651	'Alopeke	Hartman	2025/02/17	5.046	7.304	4.206	7.307

Table 2 continued on next page

Table 2 (*continued*)

TIC ID	Instrument	P.I.	Date	562 nm		832 nm	
				Contrast @ 0.1''	Contrast @ 0.5''	Contrast @ 0.1''	Contrast @ 0.5''
				yyyy/mm/dd	[mag]	[mag]	[mag]
95431211	'Alopeke	Hartman	2025/02/17	4.850	6.954	4.131	6.471
101641846	'Alopeke	Hartman	2025/02/17	4.886	7.372	4.201	6.972
113710966	'Alopeke	Burt	2020/12/04	5.150	6.920	4.488	6.537
113710966	'Alopeke	Howell	2024/09/25	5.069	7.168	4.185	6.895
116988032	'Alopeke	Burt	2020/12/02	5.083	7.007	4.750	6.988
"	"	Howell	2024/09/27	5.029	6.943	4.782	6.745
117979951	Zorro	Burt	2020/11/27	4.319	6.697	5.088	6.681
118572803	'Alopeke	Burt	2020/12/06	5.089	5.977	4.919	6.800
135656809	Zorro	Howell	2021/06/27	4.659	6.291	4.737	6.972
"	"	"	2021/07/23	—	—	4.856	6.613
141810080	Zorro	Howell	2019/12/22	3.995	6.329	4.542	6.224
"	"	Burt	2020/11/25	3.219	3.456	4.569	6.417
147407292	Zorro	Burt	2020/10/23	5.238	6.531	5.211	6.646
155315739	Zorro	Hartman	2025/01/09	4.503	5.721	4.843	6.732
156890613	'Alopeke	Hartman	2025/02/17	4.700	6.424	4.386	7.216
157364190	NESSI	Howell	2023/07/12	2.761	6.221	1.906	6.080
157966796	'Alopeke	Hartman	2025/02/17	4.541	7.490	3.978	7.128
165602000	'Alopeke	Burt	2020/08/10	5.319	7.237	4.690	6.989
"	"	Howell	2024/08/13	5.789	7.329	4.800	7.560
165602023	'Alopeke	Burt	2020/08/10	5.369	6.959	4.496	6.984
"	"	Howell	2024/08/13	5.899	7.167	4.884	7.222
166646191	'Alopeke	Hartman	2025/02/17	4.806	6.731	4.101	6.529
172954294	'Alopeke	Hartman	2025/02/14	5.588	7.234	5.225	7.044
176521059	'Alopeke	Burt	2020/12/06	5.187	6.910	4.460	6.702
179348425	Zorro	Howell	2021/07/22	—	—	4.444	6.707
189576919	NESSI	Howell	2018/11/18	2.601	6.711	1.671	5.342
202380743	'Alopeke	Hartman	2025/02/17	5.033	6.135	4.868	6.657
206686962	Zorro	Burt	2020/11/24	5.308	6.948	4.912	6.617
213041474	'Alopeke	Burt	2020/12/07	5.146	6.770	4.683	6.794
219709102	NESSI	Howell	2019/01/25	2.247	5.223	1.910	5.816
229092427	Zorro	Burt	2020/11/24	5.408	7.032	4.644	6.683
229902025	'Alopeke	Hartman	2025/02/18	6.042	7.259	5.191	6.716
231698181	Zorro	Burt	2020/10/23	5.600	6.545	5.278	6.725
238432056	'Alopeke	Burt	2020/12/06	5.034	6.944	5.244	6.635
257393898	'Alopeke	Burt	2020/12/24	5.194	6.743	4.293	6.270
"	"	Howell	2024/09/26	5.408	7.111	5.147	6.968
259237827	'Alopeke	Howell	2024/08/13	4.780	5.416	4.828	7.089
259291108	Zorro	Burt	2020/01/02	4.857	6.366	4.852	6.238
261136679	Zorro	Burt	2020/11/26	4.415	4.600	5.142	6.568
279649049	Zorro	Howell	2020/10/23	4.803	6.040	4.701	6.355
"	"	Burt	2020/11/26	4.993	6.177	4.633	6.604
"	"	Hartman	2025/01/08	4.803	6.167	4.420	6.876
"	"	"	2025/01/09	5.149	6.559	5.671	6.948
279649057	Zorro	Howell	2020/10/23	5.019	6.638	4.820	6.499
"	"	Burt	2020/11/26	5.117	6.098	4.744	6.293
283722336	'Alopeke	Burt	2020/08/04	4.583	5.917	4.089	6.025
"	"	Howell	2024/09/27	4.813	6.730	4.863	7.632
285544488	'Alopeke	Howell	2023/12/04	4.943	6.441	4.821	6.546
"	"	Hartman	2024/09/25	4.546	5.836	4.611	6.943
289673491	Zorro	Burt	2020/11/24	4.844	6.775	4.735	6.640
301051051	Zorro	Burt	2020/11/25	4.996	6.727	4.666	6.460
302158903	'Alopeke	Howell	2024/09/27	4.734	6.706	4.619	6.715
309599261	'Alopeke	Hartman	2025/02/15	5.791	7.178	5.171	6.811
311063391	'Alopeke	Hartman	2025/02/16	5.141	6.879	4.695	7.280
311092847	'Alopeke	Burt	2020/12/07	4.666	7.090	4.452	6.963
328324648	'Alopeke	Hartman	2025/02/17	4.883	6.435	4.244	7.260
332064670	NESSI	Howell	2018/11/18	2.166	4.556	1.991	5.388
343813545	NESSI	Howell	2019/01/25	2.490	5.283	2.009	6.215
"	'Alopeke	Burt	2020/12/05	5.068	6.987	4.315	6.183
"	"	Howell	2023/12/02	5.583	6.954	4.455	6.498
"	"	"	2024/09/26	5.431	7.069	4.778	7.217
355127594	'Alopeke	Hartman	2025/02/18	5.466	7.124	4.76	6.867
366661076	Zorro	Howell	2023/03/05	4.911	6.999	5.185	7.660
367631379	'Alopeke	Hartman	2025/02/17	4.914	5.845	4.814	6.578

Table 2 continued on next page

Table 3. Speckle Detected Binary Results

TIC ID	ρ	θ	Δm
-	[$''$]	[$^{\circ}$]	[mag]
259291108	0.883	63.300	7.500
367631379	0.022	2.374	0.480

NOTE—Only 832 nm filter results shown.
No companions were found in the
562 nm observations.

Table 2 (continued)

TIC ID	Instrument	P.I.	Date	562 nm		832 nm	
				Contrast @ 0.1''	Contrast @ 0.5''	Contrast @ 0.1''	Contrast @ 0.5''
-	-	-	yyyy/mm/dd	[mag]	[mag]	[mag]	[mag]
371520835	‘Alopeke	Howell	2024/03/21	4.707	5.855	4.494	7.085
”	”	”	2024/11/20	5.350	6.659	4.589	6.845
”	”	Hartman	2025/02/15	5.064	5.580	5.398	6.929
373694425	‘Alopeke	Burt	2020/12/03	4.685	5.585	4.709	6.419
”	”	Howell	2024/08/15	4.812	6.239	4.515	7.322
373765355	‘Alopeke	Hartman	2025/02/17	5.365	7.222	4.267	6.927
377415363	‘Alopeke	Howell	2019/06/07	5.465	6.880	4.719	6.737
389853353	‘Alopeke	Hartman	2025/02/17	5.037	6.794	4.790	6.751
399665349	NESSI	Howell	2019/01/23	2.594	6.313	2.022	5.827
”	‘Alopeke	”	2024/11/21	5.089	7.396	4.543	7.045
409104974	‘Alopeke	Hartman	2025/02/18	4.718	6.777	3.844	6.851
416519065	‘Alopeke	Howell	05/23/2024	4.557	5.722	3.541	6.896
”	”	”	2024/11/21	5.404	6.168	4.756	6.624
”	”	Hartman	2025/02/17	3.618	5.197	4.220	5.917
417762326	‘Alopeke	Hartman	2025/02/18	4.200	5.160	4.527	7.019
419015728	NESSI	Howell	2018/11/20	2.921	7.273	1.768	6.607
”	Zorro	Burt	2020/11/28	5.303	7.047	4.890	6.769
425935521	Zorro	Howell	2020/10/29	4.309	6.555	4.431	6.357
”	Zorro	Burt	2020/11/25	5.304	6.346	4.477	6.651
434210589	‘Alopeke	Burt	2020/12/06	5.007	6.850	4.613	6.572
437886584	‘Alopeke	Hartman	2025/02/18	5.436	7.336	4.516	7.187
441709021	NESSI	Howell	2019/01/20	2.574	5.778	2.037	5.423
445070560	‘Alopeke	Howell	2024/01/23	5.072	7.072	4.325	6.962
”	”	Hartman	2025/02/17	5.072	7.072	4.325	6.962
445258206	‘Alopeke	Burt	2020/12/03	4.610	5.135	4.960	6.514
”	”	Howell	2024/09/26	5.309	6.065	4.769	6.459
458445966	‘Alopeke	Hartman	2025/02/17	4.948	6.761	4.257	6.474
1101124558	‘Alopeke	Hartman	2025/02/18	5.591	7.151	5.172	7.039
1101124559	‘Alopeke	Hartman	2025/02/18	4.931	6.704	4.423	6.522

Table 4. Relevant Gaia Information

TIC ID	Gaia DR3 ID	R.V. Error	R.UWE	IPD_fmp	NSS	IPD_gof	RV_gof	RV_chi	RV_nb	Source	Gaia ID ₂	Gaia ID ₃	ρ_1	Δm_1	ρ_2	Δm_2
-	-	[km/s]	-	-	-	-	-	-	-	-	-	-	[mag.]	[mag.]	[mag.]	[mag.]
3962869	247360800950466688	0.12	1.03	-	0.07	-	0.33	12	-	-	-	-	-	-	-	-
89155802	798068905726303232	0.119	1.01	-	0.05	-	0.25	27	1.	798068940086479104	-	-	7.134	-5.982	-	-
11310083	5663558453071724288	0.129	0.85	-	0.01	-	0.0	32	-	-	-	-	-	-	-	-
21555479	77754360337133312	0.123	0.85	-	0.01	-	0.1	17	-	-	-	-	-	-	-	-
23989522	821455861647126656	0.115	0.8	-	0.01	-	0.71	9	-	-	-	-	-	-	-	-
3407611182744289152	0.125	0.88	-	-	0.06	-	-	-	-	-	-	-	-	-	-	-
38511251	516412076333028736	-	2.99	-	0.03	-	0.24	19	-	-	-	-	-	-	-	-
46125330	3374052988354372892	0.139	1.18	-	0.04	-	0.99	15	-	-	-	-	-	-	-	-
47346402	3400292738990117888	0.138	0.82	-	0.15	-	0.38	12	2.	3394298532176344960	-	707.219	2.693	-	-	
60716322	27194753266772416	0.124	3.27	-	0.01	-	0.01	35	1.	27194753266731552	-	11.042	-6.68	-	-	
67772871	3105919528989223340	0.12	1.94	-	0.01	-	0.01	18	2.	3105919528989223340	78.097	5.595	83.337	5.362	-	
72748794	5117974602912370432	0.126	1.07	2	0.07	-	0.04	12	-	-	-	-	-	-	-	-
80226651	338172613874753536	0.135	0.95	-	0.05	-	0.69	16	-	-	-	-	-	-	-	-
95431211	62484408880100992	0.136	1.1	-	0.09	-	0.14	21	-	-	-	-	-	-	-	-
101641846	402585071201819392	0.139	1.14	-	0.04	-	0.61	29	-	-	-	-	-	-	-	-
113710966	96331172942614528	0.126	1.26	-	0.01	-	0.14	24	-	-	-	-	-	-	-	-
116988032	436648129327098496	0.117	2.67	-	0.01	-	0.49	11	-	-	-	-	-	-	-	-
11797951	2980492338758410112	0.117	1.07	1	0.04	-	0.83	12	-	-	-	-	-	-	-	-
118572803	5104707970261890560	-	2.72	-	0.04	-	0.83	16	-	-	-	-	-	-	-	-
133656809	4345775217221521312	0.121	0.98	-	0.02	-	0.95	55	-	-	-	-	-	-	-	-
141810080	5264749303462961280	0.12	1.36	-	0.03	-	0.25	31	1.	5264749303457104384	-	3.29	-7.465	-	-	
147407292	656409119088411520	0.116	0.88	-	0.02	-	0.58	16	-	-	-	-	-	-	-	-
155315739	65536142323452800	0.133	0.93	-	0.06	-	0.56	14	-	-	-	-	-	-	-	-
156890613	974887554153340	0.122	1.11	-	0.09	-	0.23	23	-	-	-	-	-	-	-	-
157364190	1384195086792268800	0.121	0.95	-	0.04	-	0.58	12	-	-	-	-	-	-	-	-
157966796	1284237623084916480	0.123	1.18	-	0.03	-	0.92	30	-	-	-	-	-	-	-	-
165602000	187204660934556480	0.117	1.2	-	0.07	-	0.66	44	2.	1872046574983497216	-	31.593	0.684	-	-	
166646191	762815470562110464	0.131	0.96	-	0.03	-	0.78	27	-	-	-	-	-	-	-	-
163602023	1872046574983497216	0.118	0.96	1	0.01	-	0.14	17	2.	187204660934556480	-	31.593	0.684	-	-	
172954294	74634517257256384	0.122	0.94	-	0.04	-	0.0	17	2.	74634517257256384	-	134.386	8.919	-	-	
176521059	3023711269067191296	0.121	1.02	-	0.02	-	0.65	10	-	-	-	-	-	-	-	-
179348425	600953855839374336	0.122	0.94	-	0.02	-	0.53	13	2.	600953855839374336	-	14.456	7.167	-	-	
189576919	348020482735930112	0.126	7.25	-	0.01	-	0.58	12	2.	348020482735930112	-	55.618	8.531	-	-	
202380743	1661568850770761600	0.122	0.99	-	0.09	-	0.0	34	-	-	-	-	-	-	-	-
206686962	6604147121141267712	0.124	0.92	-	0.06	-	0.8	35	-	-	-	-	-	-	-	-
213041474	321146146944773376	0.121	0.97	-	0.01	-	0.42	24	-	-	-	-	-	-	-	-
219709102	1068932214258617216	0.117	0.86	-	0.02	-	0.34	18	1.	1068932214258617216	-	4.466	-3.623	-	-	
228092427	493492302838871296	0.117	1.38	-	0.02	-	0.85	14	-	-	-	-	-	-	-	-
229902025	126463041281636720	0.13	1.08	-	0.02	-	0.02	19	-	-	-	-	-	-	-	-
231698181	641255290592307840	0.129	1.15	-	0.03	-	0.67	30	-	-	-	-	-	-	-	-
238432056	2860924621205256704	0.117	0.86	-	0.01	-	0.98	22	-	-	-	-	-	-	-	-
252393898	255295564460225152	0.118	1.08	-	0.02	-	0.0	21	-	-	-	-	-	-	-	-
252393898	226161424931057664	0.128	1.68	1	0.01	-	0.21	9	-	-	-	-	-	-	-	-
252921108	640855180222368384	0.143	2.42	2	0.04	-	0.7	12	1.	640855180222368384	-	23.597	-7.357	-	-	
261136679	4623036865373793408	0.118	0.81	-	0.03	-	0.98	15	-	-	-	-	-	-	-	-
279649049	4722135642226902656	0.128	1.2	-	0.03	-	0.48	28	2.	4722135642226902656	-	309.115	0.265	-	-	

Table 4 continued on next page

Table 4 (continued)

TIC ID	Gaia DR3 ID	R.V. Error	FUWE	IPD_fmp	NSS	IPD_gof	RV_gof	RV_chi	RV_nb	Source	Gaia ID_2	Gaia ID_3	ρ_1	Δm_1	ρ_2	Δm_2
-	-	[km/s]	-	-	-	-	-	-	-	-	[']	[mag.]	[']	[mag.]	[']	[mag.]
279649057	4722111590409480064	0.122	0.98	-	-	0.02	-	0.88	23	2.	4722135642226902656	-	-	309.115	0.265	-
283722336	2009481748875806976	0.119	1.0	-	-	0.06	-	0.37	20	-	-	-	-	-	-	-
285544488	42732415301550208	0.123	1.08	-	-	0.0	-	0.7	20	-	-	-	-	-	-	-
286775491	2416611663182821120	0.128	1.69	-	-	0.02	-	0.94	28	-	-	-	-	-	-	-
301051051	4847957293278177024	0.127	1.98	-	-	0.03	-	0.98	22	-	-	-	-	-	-	-
302158903	438829629114680704	0.127	3.17	-	-	0.04	-	0.01	15	1.	438829835272390784	-	20.932	-5.157	-	-
309599261	4034171629042489088	0.122	0.88	-	-	0.03	-	0.09	14	-	-	-	-	-	-	-
311063391	263916708025623680	0.126	0.96	-	-	0.02	-	0.19	13	2.	26391674238557056	-	98.035	2.928	-	-
311092847	3263836568394170880	0.116	3.06	1	-	0.02	-	0.0	16	-	-	-	-	-	-	-
328324648	97689332344104576	0.128	1.49	-	-	0.01	-	0.08	21	-	-	-	-	-	-	-
332064670	704967037090946688	0.122	0.86	-	-	0.03	-	-	-	2.	704966762213039488	-	84.826	5.95	-	-
34881545	326930264511584940	0.148	1.34	-	-	0.03	-	0.24	30	-	-	-	-	-	-	-
355127594	714116137767540096	0.119	0.87	-	-	0.0	-	0.63	13	-	-	-	-	-	-	-
366661076	378644268048579328	0.296	2.81	-	-	0.06	-	0.09	14	-	-	-	-	-	-	-
3671631379	1146337324038514176	0.636	9.92	1	1	0.03	-	0.0	27	1.	1146337324038513536	-	13.495	-7.604	-	-
371520835	823773494718931968	0.119	0.94	-	-	0.02	-	0.98	26	-	-	-	-	-	-	-
373684425	512167948043650816	0.12	0.98	-	-	0.02	-	0.41	5	-	-	-	-	-	-	-
373763355	3936909723803446368	0.123	0.95	-	-	0.02	-	0.21	34	2.	3936909723803146496	-	7.671	2.572	-	-
377415363	1193030490492925824	0.127	1.54	-	-	0.01	-	0.94	24	-	-	-	-	-	-	-
389853353	1521686732461765888	0.124	0.83	-	-	0.02	-	0.37	21	-	-	-	-	-	-	-
399663349	328892172025503360	-	3.92	-	-	0.07	-	0.23	9	-	-	-	-	-	-	-
409104974	18877113583575504	0.12	0.89	-	-	0.01	-	0.7	17	-	-	-	-	-	-	-
416519065	85381994475694120	0.123	0.89	-	-	0.03	-	0.03	29	2.	85382094818113472	-	122.865	3.411	-	-
417762326	1092545710514654464	0.117	1.17	-	-	0.04	-	0	14	-	-	-	-	-	-	-
419015728	2452378776134477184	-	2.63	-	-	0.05	-	1.0	11	-	-	-	-	-	-	-
425935521	490010895084961248	0.129	3.21	-	-	0.12	-	0.26	6	-	-	-	-	-	-	-
43210589	280233796085105020	0.126	0.88	-	-	0.04	-	-	-	-	-	-	-	-	-	-
43788584	33197990104216512	0.131	0.98	-	-	0.06	-	0.45	13	-	-	-	-	-	-	-
441709021	1604859511344724864	0.135	3.38	-	-	0.19	-	0.31	8	2.	1604859408265509632	-	69.674	6.581	-	-
445070560	148022944258922324	0.127	2.46	-	-	0.13	-	0.2	10	-	-	-	-	-	-	-
445258206	425040000962559616	-	3.12	-	-	0.04	-	0.0	23	1.	425040000962497792	-	13.327	-3.442	-	-
458445966	153401198572555776	0.117	2.11	-	-	0.08	-	0.58	14	-	-	-	-	-	-	-
1101124558	1237090738916392704	0.124	1.1	-	-	0.05	-	0.47	24	1.	1237090738916392832	-	5.656	-1.95	-	-
1101124559	1237090738916392832	0.125	1.51	-	-	0.09	-	-	-	1.	1237090738916392704	-	5.656	-1.95	-	-

Note.—1. - El-Bachry et al. (2021), 2. - Gaia Collaboration et al. (2021a)

Table 5. Multiplicity results for 80 observed targets using speckle observations, Gaia, and literature sources

TIC ID	WDS ID	Gaia-resolved Multiple	Elevated Gaia Metrics	Speckle Detection	Lit. Source(s)	Multiplicity Status	Notes on Multiplicity
3962869	–	–	–	–	–	–	–
8915802	09357+3549	X	X	–	8.	S	Triple system. Wide companion in WDS. TIC 8915802 is marked in the Gaia NSS. Period = 27.1 days.
11310083	–	–	–	–	1., 8.	M	–
21535479	–	–	–	–	8.	S	–
23969522	–	–	–	–	8.	S	–
27136704	05074+1839	–	–	–	4.	S	Speckle finds no companion. WDS entries marked with X and U.
38511251	–	–	X	–	6.	S	–
46125330	06148+1909	–	–	–	4.	S	All components are background stars
47346402	05244+1723	X	–	–	2.	M	AB is marked as U. Wide companion confirmed by Gaia.
60716322	22467+1210	X	X	–	1.	M	No third companion with similar parallax within 500".
67772871	04153-0739	X	–	–	2.	M	Triple
72738704	–	–	X	–	8.	S	–
80226651	–	–	–	–	8.	S	Not binary according to WDS notes
95431211	10197+1928	–	–	–	4.	S	4. marks as single.
101641846	11411+3412	–	–	–	8.	S	Marked with L
113710966	01425+2016	–	–	–	6.	S	no component seen in Gaia.
116988032	03091+4937	–	X	–	6.	S	Gaia does not see either WDS companion.
117797951	–	–	X	–	6.	S	AC is marked as U.
118572803	03329-0927	–	X	–	6.	S	WDS entry marked as S.
135655809	16156-0822	–	–	–	8.	S	Marked as X in WDS.
141810080	61102-7445	X	–	–	1.	M	WDS entry marked as U.
147407292	21483-4718	–	–	–	8.	S	–
155315739	23059-3551	–	–	–	5., 9.	S	Background source detection in 9.
156890613	–	–	–	–	8.	S	–
157364190	–	–	–	–	8.	S	Marked with L and U.
157966796	14347-2945	–	–	–	8.	S	Not seen in Gaia.
165602000	21069+3845	X	–	–	6.	M	–
165602023	21069-3845	X	–	–	6.	M	–
166646191	–	–	–	–	6.	S	–
172954294	10010+3155	X	–	–	2., 8.	M	Possible Triple due to over-luminosity.
176521059	–	–	–	–	5.	S	However, no confirmed detection.
179348425	15475-3755	X	X	–	2., 5.	M	–
189578919	01368+4124	X	X	–	2., 5.	M	AC is marked as S in WDS
202380743	–	–	–	–	8.	S	–
206686962	22577-2937	–	–	–	6.	M	Fomalhaut system
213041474	–	–	–	–	6.	S	α PsA is not in Gaia
219709102	09104+6708	X	–	–	1.	M	B-C not recovered by wide binary searches.
229092427	–	–	–	–	8.	S	Second WDS entry not confirmed in Gaia
229092025	15073+2452	–	–	–	8.	S	All WDS entries marked with U.
231698181	22034-5647	–	–	–	6.	M	Part of triple with brown dwarf binary
238432056	00066-2901	–	–	–	8.	S	All other WDS entries are marked with U.

Table 5 continued on next page

Table 5 (continued)

TIC ID	WDS ID	Gaia-resolved Multiple	Elevated Gaia Metrics	Speckle Detection	Lit. Source(s)	Multiplicity Status	Notes on Multiplicity
257393898	00484+0517	—	—	—	6.	S	No companions seen in Gaia. Second WDS entry marked with U.
259237827	19324+6940	—	—	—	6.	S	No companions seen in Gaia.
259291108	22249+5748	X	X	X	1., 7.	M	Triple system with close-in companion.
261136679	—	—	—	—	5.	S	
279649049	03182+6230	X	—	—	2.	M	No close binary detected
279649057	03182+6230	X	—	—	2.	M	No close binary detected
28572336	23133+5710	—	—	—	6.	S	All WDS components marked as U.
285544488	00531+6107	—	—	—	4.	S	
289673491	—	—	—	—	8.	S	
301051051	—	—	—	—	6.	S	
302158903	02442+4914	X	X	—	1.	M	Potential Third companion BD although only seen once.
30959261	—	—	—	—	6.	S	
311063391	05413+5329	X	—	—	8.	M	All other WDS entries marked with U.;
311092847	—	—	X	—	8.	S	
328324648	07299+4940	—	—	—	4.	S	
332064670	08326+2820	X	—	—	2., 5.	M	
343815545	03194+0322	—	—	—	6.	S	WDS entries marked with U.
355127594	—	—	—	—	8.	S	
366661076	11507+0146	—	X	—	8.	S	Both WDS entries listed as L or U.
367631379	10311+8234	X	X	X	1., 3., 4.	M	Close companion detected in our speckle observations. Marked as NSS.
371520835	10114+4927	—	—	—	6.	S	No Gaia confirmation of companions.
373694425	01477+6351	—	—	—	8.	S	Both WDS entries marked with L or U.
377763355	13169+1701	X	—	—	5.	M	
377415363	15565+1540	—	—	—	8.	S	WDS entries marked with L or S.
389853353	05191+4006	—	X	—	8.	S	All WDS entries are chance alignments
399663349	04498+0658	—	—	—	6.	S	Potential BD companions; Lefebvre et al. (2007).
409104974	—	—	—	—	8.	S	Other WDS entries are marked with U.
416518065	10306+5559	X	—	—	2.	M	Second WDS entry is U
417763326	—	—	—	—	8.	S	
419011728	01441+1556	—	X	—	6.	S	WDS entry marked with L.
425933521	—	X	—	—	6.	S	AB entry marked with U.
43210589	00394+2115	—	—	—	5.	M	C is brown dwarf companion.
437886584	06164+1216	—	—	—	4.	S	WDS reports two companions. Gaia does not detect these.
441709021	14252+5151	X	X	—	2.	M	4. lists the target as single Wide Companion
445070560	13119+7753	—	X	—	6.	S	WDS entry marked with U.
445253206	00491+5749	X	X	—	6.	M	Wide companion
45845966	12337+1121	—	X	—	8.	S	Other WDS entries marked with U; L; and S
1101124558	14514+1906	X	—	—	6.	M	WDS entries marked with X or U.
1101124559	14514+1906	X	—	—	6.	M	Other WDS entries marked with U
							Other WDS entries marked with U

Note—1. - El-Badry et al. (2021). 2. - Gaia Collaboration et al. (2021a), 3. - Gaia Collaboration et al. (2023a), 4. - Golovin et al. (2023), 5. - González-Payo et al. (2024), 6. - González-Payo et al. (2025), 7. - Kane et al. (2019), 8. - Kirkpatrick et al. (2024), 9. - Ward-Duong et al. (2015)